VEGF OVEREXPRESSION IN ATHEROSCLEROSIS

INVESTIGATING THE EFFECTS OF VEGF OVEREXPRESSION ON HYPERGLYCEMIA ACCELERATED ATHEROSCLEROSIS

By: RANGANA TALPE GURUGE, HBSc

A Thesis Submitted to the School of Graduate Studies in Partial Fulfilment of the Requirements for the Degree Master of Science

McMaster University MASTER OF SCIENCE (2022) Hamilton, Ontario

(Medical Sciences)

TITLE: Investigating the effects of VEGF overexpression on hyperglycemia accelerated atherosclerosis

AUTHOR: Rangana Talpe Guruge, HBSc (University of Western Ontario)

SUPERVISOR: Dr. Geoff H. Werstuck

NUMBER OF PAGES: xviii, 111

LAY ABSTRACT

Diabetes is a chronic disease characterized by high blood sugar. A serious complication of diabetes is a higher risk for heart disease. However, we still do not entirely understand why this occurs. One of the causes of heart disease is the buildup of fats in the walls of large arteries. Mice with diabetes have fewer new small blood vessels supplying the wall of large arteries. We believe this is because of the lower production of a protein called vascular endothelial growth factor (VEGF). This study demonstrates that in diabetic mice, increasing VEGF during the early stages of fat buildup slows down the further progression of the disease. Future work on this project will focus on understanding how this happens. With the increasing prevalence of diabetes, understanding and developing new treatments for diabetic patients have never been more important.

ABSTRACT

Diabetes mellitus is a chronic disease that can lead to severe complications, including an increased risk of cardiovascular disease. The underlying mechanisms that link diabetes to the development of vascular complications are not fully understood. Previous research from our lab has shown that hyperglycemic mice have accelerated atherosclerosis progression, in addition to increased arterial hypoxia, inflammation, and expression of hypoxia-inducible factor 1 alpha (HIF1-α), a transcription factor for genes involved in angiogenesis. However, impaired signalling through the HIF1-α pathway is evidenced by reduced vascular endothelial growth factor (VEGF), VEGF receptor 2 (VEGFR2) and impaired neovascularization of the vasa vasorum – a microvascular network of capillaries that supply the walls of large arteries. We hypothesize that impaired VEGF expression contributes to the accelerated development of atherosclerosis in hyperglycemia. The objective of this study is to test a model of VEGF overexpression on atherosclerosis in hyperglycemia. A macrophage-specific inducible system for VEGF transgene overexpression was established using Cre-Lox technology. Triple mutant $apoE^{-/-}$ROSA26-FLOXSTOP-$VEGF_{164}^{tg/0}$ $CSF1R\text{-}iCRE^{tg/0}$ mice were generated in a C57BL/6 background. Hyperglycemia was induced in half of the mice with streptozotocin. Macrophage-specific Cre recombinase was activated with tamoxifen at early and later stages of atherosclerosis, and hearts/aortas were harvested at 15 weeks of age. Lesion volume and expression of key factors in hypoxia-mediated

angiogenesis were quantified. Our results demonstrate that overexpression of VEGF during early atherosclerosis progression reduces plaque volume and expression of the hypoxic marker, HIF-1α, in female mice. Understanding the effects of VEGF expression on lesion development will help delineate the biochemical pathways that link diabetes and cardiovascular disease. Validation of this mechanism may lead to novel and more effective strategies to treat/prevent diabetic cardiovascular disease.

ACKNOWLEDGEMENTS

The completion of this project would not have been possible without the support of numerous people. I would like to thank my supervisor, Dr. Geoff Werstuck, who gave me the opportunity to pursue my interests in medical research. His guidance and consistent confidence in my abilities helped me navigate the ups and downs of scientific research and become a more resilient and knowledgeable researcher. I would also like to thank my committee members, Dr. Jonathan Schertzer, and Dr. Hertzel Gerstein, for their time contributing to the progress of my project. They shared unique perspectives that allowed me to gain a broader understanding of my research topic.

Next, I would like to thank the past and present members of the Werstuck lab, including Alexandra Bruton, Dr. Daniel Venegas-Pino, Dr. Monica De Paoli, Dr. Sarvatit Patel, Dr. Lauren Mastrogiacomo, and Sophie Enright. I am thankful for their time and patience in teaching me invaluable laboratory methods and techniques. Their constant support and friendship brought assurance and laughter to even the most challenging times. I would also like to acknowledge Kiara Takeda for their hard work assisting me in parts of this project.

Lastly, I would like to express my gratitude to my support system outside of academia for their unwavering love and support. I am continually thankful for my parents, who brought me to Canada and whose countless sacrifices have given me the opportunity to pursue my academic goals, and my siblings, who

have guided me throughout my life. I am grateful for my partner, Matthew Price, who has been my closest support during my graduate studies. Finally, I would like to thank my dear friends, relatives, and Sri Lankan community in Canada for their encouragement throughout the years.

TABLE OF CONTENTS

LIST OF FIGURES

LIST OF TABLES

LIST OF ABBREVIATIONS AND SYMBOLS

AGEs	Advanced Glycation End Products
ANOVA	Analysis Of Variance
apoE	Apolipoprotein E
$apoE^{-/-}$	Apolipoprotein E Knockout
$apoE^{+/-}$	Apolipoprotein E Heterozygous
ARD1	Arrest Defective 1
ATP	Adenosine 5′-Triphosphate
CBP	CREB-Binding Protein
cDNA	Complimentary Deoxyribonucleic Acid
CSF1R	Colony Stimulating Factor 1 Receptor
$CSF1R\text{-}iCRE^{tg/0}$	Csf1r-Cre/Esr1* Single Gene Knock-In
CVD	Cardiovascular Disease
DAPI	4′,6-diamidino-2-phenylindole
DM	Diabetes Mellitus
DNA	Deoxyribonucleic Acid
ECM	Extracellular Matrix
EDTA	Ethylenediaminetetraacetic Acid
ELISA	Enzyme-Linked Immunosorbent Assay
FIH-1	Factor Inhibiting HIF-1
FVB	Friend Leukemia Virus B
GAPDH	Glyceraldehyde 3-Phosphate Dehydrogenase
HbA1c	Hemoglobin A1C
HDL	High Density Lipoprotein
HG	Hyperglycemic
HIF	Hypoxia Inducible Factor

IgG	Immunoglobulin G
IP	Intraperitoneal
LDL	Low Density Lipoprotein
mRNA	Messenger Ribonucleic Acid
NG	Normoglycemic
NRP1	Neuropilin-1
NS	Not significant
ODD	Oxygen Degradation Domain
OHT	4-Hydroxytamoxifen
oxLDL	Oxidized Low Density Lipoprotein
PBS	Phosphate Buffered Saline
PCR	Polymerase Chain Reaction
PHD	Prolyl Hydroxylase
PIGF	Placenta Growth Factor
PK	Proteinase K
RT qPCR	Reverse Transcription Quantitative PCR
SDS-PAGE	Sodium Dodecyl Sulfate Polyacrylamide Gel Electrophoresis
SEM	Standard Error of the Mean
SMC	Smooth Muscle Cell
STZ	Streptozotocin
TAD	Terminal Transactivation Domain
TAM	Tamoxifen
TCA	Tricarboxylic Acid
VEGF	Vascular Endothelial Growth Factor
VEGFR1	Vascular Endothelial Growth Factor Receptor 1
VEGFR2	Vascular Endothelial Growth Factor Receptor 2

$VEGF^{tg/0}$	ROSA26-FLOXSTOP-VEGF164 Single Gene Knock-In
$VEGF^{tg/tg}$	ROSA26-FLOXSTOP-$VEGF_{164}$ Double Gene Knock-In
VHL	Von Hippel-Lindau Protein
VLDL	Very Low-Density Lipoproteins
vWF	von Willebrand Factor
WT	Wildtype

DECLARATION OF ACADEMIC ACHIEVEMENT

This study has characterized a novel atherosclerosis-prone mouse strain that has been genetically modified to permit inducible, macrophage-specific VEGF overexpression by injecting the small molecule, tamoxifen. Analysis of normoglycemic and hyperglycemic mice reveal that transient VEGF overexpression during the early stages of atherosclerosis progression is sufficient to reduce atherosclerotic plaque buildup and decrease hypoxia within the aorta of female hyperglycemic mice.

Experiments conducted in this study were completed by Rangana Talpe Guruge with some assistance. The novel mouse model and breeding scheme was created by Dr. Werstuck, Dr. Venegas-Pino, and Dr. Peter Shi and maintained by Rangana Talpe Guruge during the course of this project. The experimental design testing the effects of VEGF overexpression at two different time-points was created by Dr. Werstuck and Alexandra Bruton. Collection of samples was initiated by Alexandra Bruton, but a predominantly completed by Rangana Talpe Guruge. All murine samples were prepared and processed by Rangana Talpe Guruge. Kiara Takeda assisted with sectioning and staining of male samples.

1. INTRODUCTION

1.1 Diabetes Mellitus

1.1.1 Definitions and Diagnosis

Diabetes Mellitus (DM) is a heterogeneous metabolic disorder characterized by chronic hyperglycemia [1]. An estimated 536.6 million adults worldwide live with DM, which is projected to increase to 783.2 million by 2045 [2]. There are two main types of DM: type 1 and type 2. In Canada, 10% of adults have been diagnosed with either type 1 or type 2 DM [3]. Type 1 DM results from impaired β-cell function leading to insulin deficiency and includes people with acute onset autoimmune disorder and cases where the cause of the β-cell destruction is unknown. Type 1 DM is generally treated with the immediate introduction of exogenous insulin. Type 2 DM is more common, representing about 90% of DM diagnoses, and is associated with insulin resistance that exceeds the beta cells' capacity to secrete insulin. Treatment approaches vary but generally involve the initial use of noninsulin drugs containing antihyperglycemic agents (i.e., metformin); however, exogenous insulin may be introduced as the disease progresses. Other less common types of DM include gestational DM, monogenic DM syndromes, DM caused by diseases of the exocrine pancreas, and drug-induced DM [1,4,5]. While many underlying causes

of impaired insulin action exist, all forms of DM present with elevated blood glucose.

Due to the heterogeneous nature of the disease, differentiating between type 1, type 2, and other causes of DM is sometimes challenging [6]. Clinical features such as the age of onset, weight, islet autoantibodies, c-peptide, insulin production, and family history of DM are considered when diagnosing DM [1]. However, initially, a blood test measuring plasma glucose and/or glycated hemoglobin (HbA1c) is used to diagnose DM since all types of DM are characterized by hyperglycemia. Plasma glucose is measured either after a fasting period (usually at least 8 hours) or measured randomly. A diagnosis of DM is conferred when fasting plasma glucose is consistently ≥ 7.0mmol/L or random plasma glucose is ≥ 11.1mmol/L. Glucose tolerance can be measured by oral administration of 75g of glucose and measuring plasma glucose 2 hours later. DM is diagnosed when the 2-hour post-prandial glucose levels are ≥ 11.1mmol/L. HbA1c is a less sensitive diagnostic measure than glucose tests but is advantageous in that it is not dependent on the time of day or short-term variations of blood glucose, as it is a measure of the average plasma glucose over 2 to 3 months. The accuracy of HbA1c can be affected by certain medical conditions, ethnicity, age, altitude, pregnancy, and other factors. When appropriate, values of HbA1c ≥ 6.5% are indicative of DM [1]. Other tests are used to differentiate between the different types of DM.

If patients have test results that approach but do not meet the DM thresholds, they may be diagnosed with pre-diabetes, a condition where one is at high risk of developing DM. Pre-diabetes is diagnosed when fasting plasma glucose, glucose tolerance test, or HbA1c levels range between 6.1-6.9 mmol/L, 7.8-11 mmol/l, or 6.0-6.4%, respectively [5].

1.1.2 Hyperglycemia

Insulin is a peptide hormone produced in beta cells, located in the core of the islets of Langerhans, in the endocrine component of the pancreas [7]. In normal glucose homeostasis, increases in plasma glucose activate insulin production and release from pancreatic beta cells, stimulating glucose uptake from the blood while suppressing endogenous glucose production. When blood glucose levels rise, glucose molecules enter beta cells and are used to produce ATP in the mitochondria. The increase in cellular ATP closes potassium ion channels and opens calcium ion channels creating a shift in the electrical equilibrium, which activates insulin release from the beta cells. Diabetic patients have impaired insulin secretion and/or insulin resistance along with hyperglycemia in varying severity [8].

In type 1 DM, the immune system targets components of beta cells leading to their destruction. This results in significantly reduced insulin production and impaired glucose clearance from the blood, resulting in hyperglycemia. The onset

of type 2 DM is more gradual, and many factors, including insulin resistance, contribute to elevated blood glucose [8].

1.1.3 Vascular Complications of Diabetes Mellitus

DM increases the risk of complications in many organs due to the effects of hyperglycemia and other associated metabolic disorders, including dyslipidemia and insulin resistance, on the vasculature. In fact, all complications of diabetes can be attributed to abnormalities in the structure, growth and/or function of blood vessels. Diabetic complications can be categorized as microvascular or macrovascular, although treatment is provided based on the affected organ and not the associated vascular category. Traditionally, micro- and macrovascular complications of DM have been regarded as different and independent conditions [9].

The most common microvascular complications of DM include retinopathy, nephropathy and neuropathy [9]. In fact, the diagnostic criterium for DM is set at a glycemic level above which patients are at significantly elevated risk for retinopathy [1]. Macrovascular complications of DM include atherosclerosis, which occurs in the large and medium arteries, in areas of curvatures and/or bifurcations [10]. Atherosclerosis, the buildup of plaques on artery walls, is present in most patients with cardiovascular disease (CVD) [11]. The risk of CVD,

such as coronary heart disease and stroke, is increased by 2-4-fold in patients diagnosed with DM [12].

While the pathologies associated with micro- and macrovascular complications of diabetes are regarded as different diseases, there are striking correlations between these disorders. For instance, many studies show that diabetic microangiopathies, like proliferative retinopathy and nephropathy, increase the risk of cardiovascular events [13]. Analysis of several studies found that diabetic retinopathy is associated with a 1.7-fold increased risk for cardiovascular events [14]. These associations may suggest that these distinct vascular disorders are, in fact, linked mechanistically and that perhaps the key to understanding macrovascular complications of diabetes, like CVD, is to study microangiopathies.

Chronic hyperglycemia in diabetes affects the ability of some cells to maintain intracellular glucose homeostasis. Endothelial cells are unable to reduce glucose transport into the cell when exposed to hyperglycemia [15]. Elevated concentrations of intracellular glucose can disrupt many critical molecular pathways within the cell. In the mitochondria, higher levels of glucose are oxidized by tricarboxylic acid (TCA), disrupting the electron transport chain, and leading to electron donation to molecular oxygen, creating superoxide [16,17]. Hyperglycemia-induced superoxides decrease the activity of glyceraldehyde 3-phosphate dehydrogenase (GAPDH), thereby increasing glycolytic intermediates

upstream of GAPDH [15,18]. These intermediates are precursors or initiators of critical pathways, which are disrupted due to dysglycemia. Hyperglycemia increases polyol pathway flux which increases the susceptibility to intracellular oxidative stress [15,16]. Elevated concentrations of glucose increase the formation of advanced glycation end products (AGEs), which damages cells by modifying proteins involved in the regulation of gene transcription, modifying extracellular matrix molecules and modifying circulating proteins such as albumin [15]. High glucose in the cell activates protein kinase C isoforms that regulate the expression of genes involved in blood flow abnormalities, vascular permeability angiogenesis, capillary occlusion, vascular occlusion, and pro-inflammatory gene expression [15,17,19]. Hyperglycemia increases hexosamine pathway flux resulting in pathologic changes in protein modification and gene expression [15]. The disruption of these pathways contributes to the development of both microvascular and macrovascular diseases by inducing and accelerating vascular dysfunction [9,15].

1.2 Vasculature and Atherosclerosis

1.2.1 Atherogenesis

Artery walls are composed of three distinct layers: the tunica intima, lined with endothelial cells that interact directly with the blood; the tunica media consisting of smooth muscle cells (SMCs) that provide strength and elasticity;

and the outer tunica adventitia providing general support of the vessel. Numerous seminal investigations support a unified canonical atherosclerosis theory, which describes atherogenesis as a lipid-driven macrovascular process initiated by endothelial dysfunction (**Figure 1**) [11,20–26]. In this model, local inflammation induced by elevated low-density lipoprotein (LDL) levels activates endothelial cells to allow monocytes and LDL into the subintimal space [20,21]. Within the intima, monocytes differentiate into macrophages, and LDL becomes oxidized (oxLDL) [22]. OxLDLs are taken up by macrophages, leading to foam cell formation [22]. In the early stages of atherogenesis, the foam cells form fatty streaks in the arterial wall [23,24]. In later stages of atherogenesis, macrophages secrete chemokines that induce SMCs to migrate from the tunica media to the tunica intima. Intimal SMCs proliferate and synthesize extracellular matrix proteins, which form a fibrotic cap over the developing plaque [25]. The excessive accumulation of intracellular lipids in foam cells results in foam cell apoptosis which accumulates in the arterial wall, forming an acellular necrotic core [11,26].

While the canonical atherosclerosis model is well supported, it does not explain why or how atherosclerosis progresses when dyslipidemia is absent. In a study of participants lacking CVD risk factors, like dyslipidemia, subclinical atherosclerosis was present in approximately 50% of the participants [27]. An alternative theory, the anoxemia atherosclerosis model, postulates that oxygen imbalance in the arterial wall is a critical factor in atherogenesis [28]. Inflammation is characterized by increased oxygen consumption, and it has been

demonstrated that hypoxia is present in the arterial wall where lesions develop. However, the molecular mechanisms that link hypoxia and atherogenesis have yet to be fully explained [28].

Figure 1: Canonical theory of atherosclerosis. (Figure adapted from "Atherosclerotic Plaque Characterization Methods Based on Coronary Imaging", 2017) [29] **1.** Atherosclerosis initiates at sites of endothelial injury. Local inflammation induced by high plasma LDL levels causes endothelial cells to express adhesion molecules. **2.** This attracts monocytes to the artery wall that then migrate into the intima. Changes in endothelial permeability also facilitate LDL entry into the subendothelial space. **3.** Within the intima, monocytes differentiate into macrophages. **4.** Inside the intima, LDL is prone to oxidation. **5.** Chemokines secreted by macrophages induce smooth muscle cells (SMCs) to migrate from the tunica media to the tunica intima. **6.** Macrophages take up oxidized LDL, leading to foam cell formation. **7.** The excessive accumulation of intracellular lipids in foam cells becomes cytotoxic, resulting in foam cell apoptosis **8.** Extracellular lipid cholesterol deposits accumulate in the arterial wall. Intimal SMCs proliferate and synthesize extracellular matrix (ECM) proteins which contribute to the formation of a fibrotic cap over the developing plaque. Over time, these processes result in advanced plaque consisting of a necrotic lipid core stabilized by a fibrotic cap. **9.** As atherogenesis progresses, the plaque may become unstable, resulting in plaque rupture and thrombus formation.

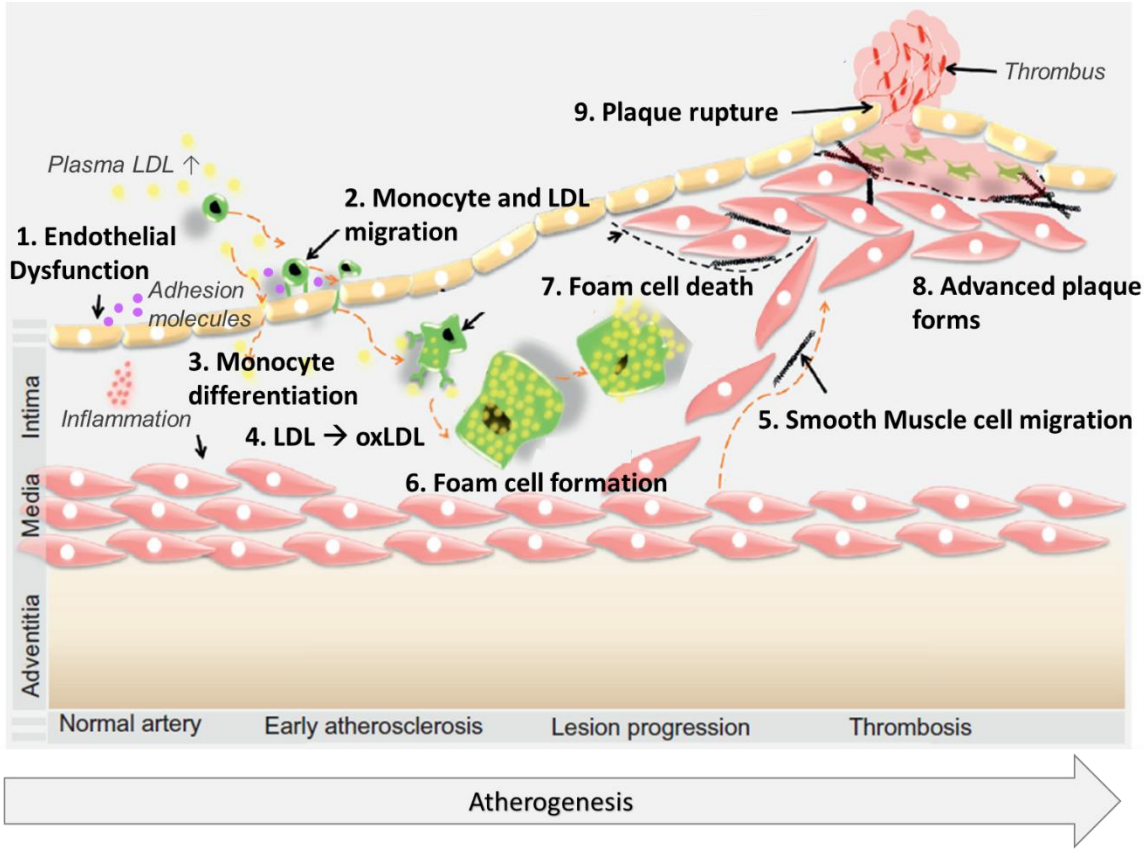
Thrombus
9. Plaque rupture
Plasma LDL ↑
2. Monocyte and LDL migration
1. Endothelial Dysfunction
Adhesion molecules
7. Foam cell death
8. Advanced plaque forms
3. Monocyte differentiation
Inflammation
4. LDL → oxLDL
5. Smooth Muscle cell migration
6. Foam cell formation
Intima
Media
Adventitia
Normal artery
Early atherosclerosis
Lesion progression
Thrombosis
Atherogenesis

1.2.2 Vasa Vasorum

The vasa vasorum is a microvascular capillary bed that supplies oxygen to the walls of large arteries (**Figure 2**). The name derives from Latin, meaning "vessels of the vessels," representing the region where microvasculature and macrovasculature meet. The walls of small vessels use diffusion to obtain nutrients and remove waste. However, cells within the wall of large vessels (luminal diameter greater than 0.5mm) and thick vessel walls (greater than 29-cell layers) cannot depend on diffusion alone and need arterial vasa vasorum to supply oxygen and nutrients and venous vasa vasorum to remove cellular waste [30]. Thus, the vasa vasorum plays an essential role in the function of a healthy artery wall.

Observational studies indicate that the vasa vasorum is dynamic during atherosclerosis. However, it is unclear if changes to the vasa vasorum promote atherosclerosis or if changes to the vasa vasorum are a reaction to atherogenesis [31].

Endothelial injury associated with the initiation of atherosclerosis can induce vasa vasorum neovascularization [32,33]. This expansion of the microvasculature may provide better access for proinflammatory and proatherogenic components to the arterial wall, thus accelerating the progression of atherosclerosis. Vasa vasorum neovascularization may also play a key role in atherosclerosis progression by creating a positive feedback loop in response to

hypoxia, in which localized hypoxia induces vasa vasorum expansion, allowing for the accumulation of proinflammatory cells, triggering the proliferation of smooth muscle cells, vessel wall thickening and hypoxia, further stimulating neovascularization of vasa vasorum [30]. This rapid expansion of microvessels can result in the production of unstable and possibly leaky vessels that allow for extravasation of blood, and deposition of lipoprotein-cholesterol and macrophages in plaques, creating plaques vulnerable to rupture [33].

However, a lack of vasa vasorum expansion can also be detrimental. A functioning vasa vasorum is essential for large arteries and thickening vessel walls to facilitate the effective removal of inflammatory elements and permit efficient reverse cholesterol transport from the cells of the artery wall [30]. Vasa vasorum density in atherosclerotic plaques is increased under some vascular disease states like hypertension and hypercholesterolemia but decreased in hyperglycemic mice [34–37]. Our studies in diabetic apolipoprotein-E knockout ($apoE^{-/-}$) mice have demonstrated that while there is an increase in arterial hypoxia and vascular inflammation during atherosclerotic progression, vasa vasorum neovascularization was impaired compared to normoglycemic controls. Staining of the aortic sinus showed an increase in hypoxia marker (hypoxia-inducible factor 1-alpha, HIF-1α), but unexpectedly, a significant decrease in angiogenesis stimulator (vascular endothelial growth factor, VEGF) in hyperglycemic mice, compared to normoglycemic controls [36,37]. Significantly, a similar deficiency in vasa vasorum density was observed in the coronary arteries

of deceased patients with diabetes relative to non-diabetic controls [38]. These findings highlight a gap in our understanding of the vasa vasorum under hyperglycemia.

Figure 2: The structure of an artery with vasa vasorum. (Figure adapted from, “Mathematical Modeling and Numerical Simulation of Atherosclerosis Based on a Novel Surgeon’s View”, 2021) [39]

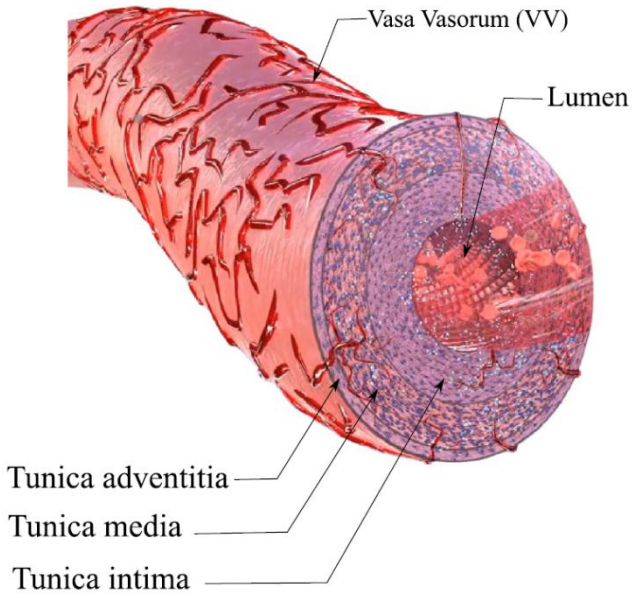
Vasa Vasorum (VV)
Lumen
Tunica adventitia
Tunica media
Tunica intima

1.2.3 Key Factors in Hypoxic Angiogenesis

Vasa vasorum neovascularization is induced by hypoxia via the hypoxia-inducible factor (HIF) complex. HIF functions by forming an α,β-heterodimer transcription factor in response to hypoxia to promote angiogenesis (**Figure 3**) [40]. HIF-1α is regulated by oxygen-dependent prolyl hydroxylase enzymes (PHDs). Under normoxic conditions, the presence of oxygen allows HIF-1α to be hydroxylated by PHDs and marked for degradation through post-translational modification. In addition, factor inhibiting HIF-1 (FIH-1) hydroxylates the C terminal transactivation domain of HIF-1α, preventing interaction with cofactors such as p300/CREB-binding protein (CBP) [41]. This prevents the formation of functional HIF transcription factors, and thus angiogenesis is inhibited. Under hypoxic conditions, hydroxylation by PHDs is reduced, and HIF-1α is stabilized, allowing the formation of a heterodimer with HIF-1β and cofactors. HIF then translocates to the nucleus, where it binds to hypoxia response elements within promoters of hypoxia-inducible genes to increase the expression of genes involved in angiogenesis [40] including VEGF, VEGF-receptor 1 (VEGFR1) and VEGF-receptor 2(VEGFR2) [42]. Dysregulation of HIF complex signalling has been implicated in the progression of atherosclerosis [42].

VEGF represents a family of proteins, including VEGF-A, VEGF-B, VEGF-C, VEGF-D, VEGF-E, and P1GF (placenta growth factor), produced in endothelial cells, macrophages and various other cell types [43,44]. VEGF-A is

the most comprehensively studied factor and has been shown to play an important role in vascular development. The human VEGF-A gene has eight exons and seven introns. Alternative splicing of the VEGF gene gives rise to nine known isoforms that play distinct roles in vascular patterning and arterial development. The corresponding murine isoforms are one amino acid shorter. The human VEGF-A_{165}a, and corresponding murine VEGF-A_{164}a isoform, are prominently expressed in pathological angiogenesis and provide long- and short-range cues for directional migration of vessel growth. VEGF-$A_{164/165}$a is regulated by two receptor tyrosine kinases, VEGFR1 and VEGFR2. VEGFR2 is the primary receptor, allowing for VEGF-$A_{164/165}$a mediated mitosis, angiogenesis, and enhancement of vessel permeability. Neuropilin-1 (NRP1) is a coreceptor for VEGFR2 and enhances the binding of VEGF-A to VEGFR2. The VEGF-$A_{164/165}$b is an anti-angiogenesis isoform that also binds to VEGFR2 with the same affinity as VEGF-$A_{164/165}$a but does not stimulate the downstream effects due to inhibiting the binding of NRP1 to VEGFR2. VEGF-$A_{164/165}$b is the dominant form expressed at basal levels in normal tissues [43–45].

The effect of DM on VEGF expression is associated with the pathogenesis of specific complications. VEGF expression is increased in some conditions, like advanced diabetic nephropathy and retinopathy, and decreased in others, like diabetic atherosclerotic lesions and the ventricles of diabetic patients [36,37,46,47]. In addition, VEGF expression and angiogenesis varies during early and late stages of some complications of DM. In apo$E^{-/-}$ mice, there is a

deficiency in the density of retinal microvessels soon after STZ-induced hyperglycemia followed by a significant increase in retinal microvessels at later stages of hyperglycemia[36]. These observations present a gap in the understanding of the effects of DM on VEGF expression.

Modulation of VEGF has been explored as a therapeutic strategy for treating many diseases. Murine models with increased VEGF expression or exogenous administration of VEGF have shown benefits such as decelerating the progression of erythroleukemia, protecting neurons from ischaemic cell death, and preventing hyperglycemia-induced vasculopathy in murine conceptuses [48–50]. The stage in disease progression in which VEGF is overexpressed is also critical. Increasing VEGF in mice has been shown to either worsen or rescue oxygen-induced retinopathy depending on which phase of disease progression the overexpression was administered or induced [51]. Within hyperglycemic mice, vessel formation is affected differently depending on the tissue/organ. When excessive neovascularization is observed, like in diabetic retinopathy, diabetic nephropathy and normoglycemic atherosclerosis, inhibition of VEGF can reduce the progression of the disease [52–54]. Similarly, the application of a topical VEGF treatment has been shown to improve wound healing in diabetic mice, a condition characterized by impaired neovascularization, much like diabetic atherosclerosis [55].

The effects of VEGF overexpression/exogenous VEGF delivery have been studied in mouse models. VEGF-C, part of the VEGF family, is a secretory

glycoprotein that regulates the physiological and pathological proliferation of lymphatic vessels [56]. Male transgenic FVB mice expressing epidermal keratinocyte-specific human VEGF-C were shown to develop insulin resistance and adipocyte hypertrophy compared to wild-type controls. This may be due to the preferential recruitment of pro-inflammatory macrophages by VEGF-C to subcutaneous white adipose tissue [57]. Within arteries, delivery of VEGF-C via F8 conjugate has been found to stabilize atherosclerotic lesions in female apoE$^{-/-}$ mice. While lesion size was not affected, a reduction in necrotic core size, thickening of the fibrous caps and expansion of collagen content within the fibrous caps were found. VEGF-C delivery also showed positive effects in improving SMC survival via the reduction of lipid accumulation within intimal SMCs [58]. Additionally, a study of arterial injury in apoE$^{-/-}$ male mice showed that delivery of human VEGF-A$_{165}$ via modified murine macrophages successfully attenuates neointima formation and accelerates re-endothelialization [59]. However, no studies have been reported analyzing the effects of VEGF-A overexpression in a diabetic atherosclerotic mouse model.

Figure 3: Hypoxia inducible factor under normal oxygen and hypoxic conditions. (Created with BioRender) The hypoxia inducible factor (HIF) is an α,β-heterodimer transcription factor, that forms in response to hypoxia to promote angiogenesis. **A.** Under normal oxygen conditions, the oxygen dependent degradation domain (ODD) of HIF-1α is hydroxylated by prolyl hydroxylase enzymes (PHDs) and acetylated by arrest defective 1 (ARD1) acetyltransferase. Oxygen is required for hydroxylation and expression of ARD1. These processes facilitate the binding of the von Hippel-Lindau protein (VHL) to the ODD domain, triggering rapid degradation via the ubiquitin-proteasome pathway. In addition, factor inhibiting HIF-1 (FIH-1) hydroxylates the C terminal transactivation domain (TAD) of HIF-1α, preventing interaction with cofactors such as p300/CREB-binding protein (CBP) [40]. This prevents the formation of functional HIF transcription factors, and thus angiogenesis is inhibited. **B.** Under hypoxic conditions, the availability of oxygen for hydroxylation by PHDs and FIH-1 is reduced, and expression of ARD1 is decreased, allowing the formation of the HIF complex consisting of the HIF-1α/HIF-1β heterodimer and cofactors. The HIF complex then translocates to the nucleus, where it binds to hypoxia response elements (HREs) within promoters of hypoxia-inducible genes to increase the expression of genes involved in angiogenesis, including VEGF, VEGF-receptor 1 and VEGF-receptor 2.

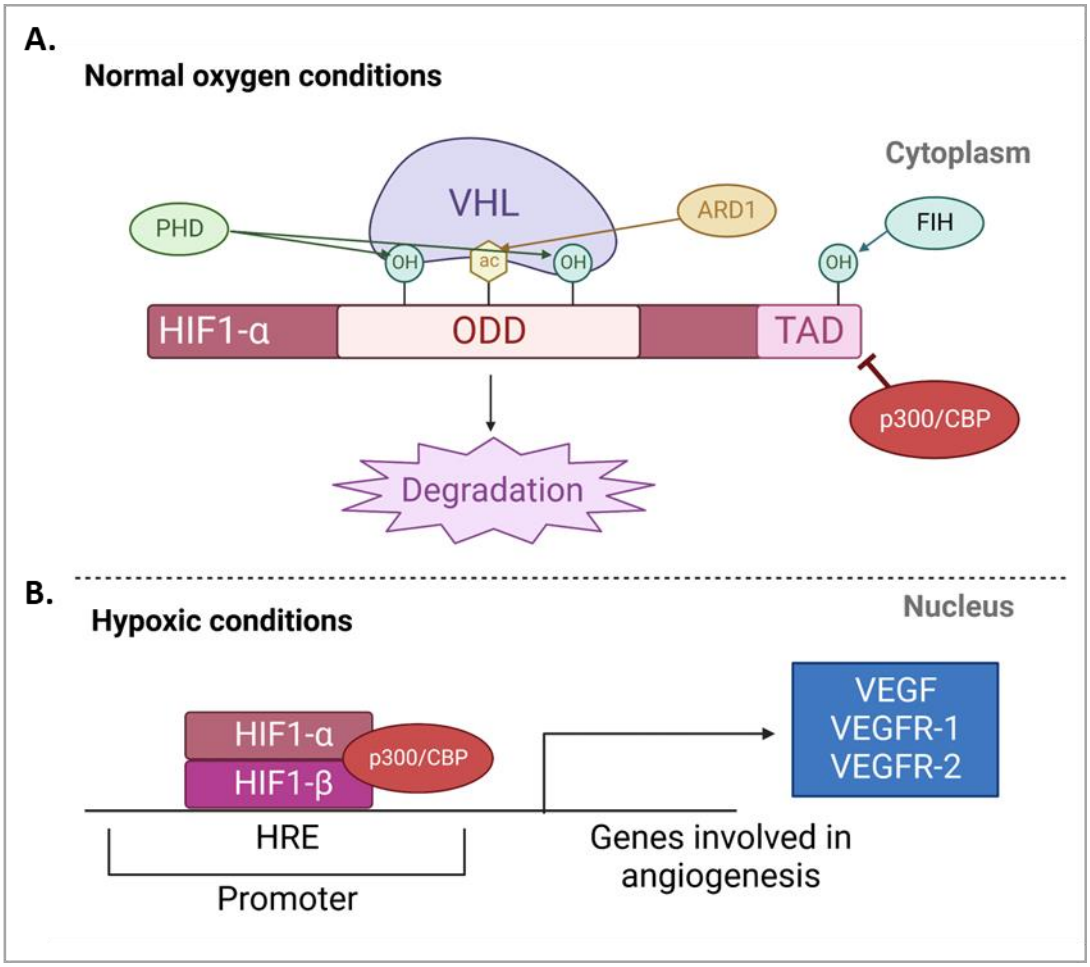
A.
Normal oxygen conditions
Cytoplasm
VHL
PHD
ARD1
FIH
OH
ac
OH
OH
HIF1-α
ODD
TAD
p300/CBP
Degradation
B.
Nucleus
Hypoxic conditions
HIF1-α
HIF1-β
p300/CBP
VEGF
VEGFR-1
VEGFR-2
HRE
Promoter
Genes involved in
angiogenesis

2. RESEARCH HYPOTHESIS

Previous studies in our lab have demonstrated that hyperglycemic mice have accelerated atherosclerotic progression, increased vascular inflammation, and increased hypoxia (and HIF-1α), but impaired neovascularization of the vasa vasorum compared to normoglycemic controls. In this model, the increased levels of HIF-1α did not correspond with an increase in VEGF-A expression [36,37].

We <u>hypothesize</u> that impaired neovascularization contributes to vascular hypoxia and accelerated development of atherosclerosis in hyperglycemia.

A novel atherosclerotic macrophage-specific inducible Cre VEGF mouse model has been established and will be used to study the effects of atherogenesis under normoglycemic and hyperglycemic conditions.

3. METHODS

3.1 Developing the Atherosclerotic Macrophage-Specific Inducible Cre VEGF Mouse Model

The mouse model we used for this project will have three genetic alterations, initially carried by three separate mice colonies and crossed to create our final experimental and control mice (**Figure 4**).

3.1.1 Apolipoprotein E

Humans transport a majority of cholesterol in LDL particles. LDL cholesterol is an independent risk factor for atherosclerosis and CVD. Wild-type mice primarily transport cholesterol in HDL particles and have low levels of LDL and very low-density lipoproteins (VLDL) remnants. This high HDL/LDL ratio is protective against lipid dysregulation and atherosclerosis development even when the mouse is fed a high-fat diet. Artificially shifting the HDL/LDL ratio in mice so that it is more similar to humans is an effective method to induce atherosclerosis and the development of lesions similar to those seen in humans [54].

Apolipoproteins are structural glycoprotein components of lipoprotein particles involved in lipoprotein transport [55,60]. Specifically, apolipoprotein E (apoE) is synthesized in the liver and constitutes the primary ligand for the LDL

receptor-mediated removal of triglyceride- and cholesterol-rich lipoproteins from the blood [60]. Macrophages also produce apoE in various tissues, including in atherosclerotic lesions [61].

ApoE knockout (apoE $^{-/-}$) mice have targeted mutations in the apoE gene resulting in an apoE deficiency [62]. ApoE$^{-/-}$ mice spontaneously develop severe hypercholesterolemia (≈ 400 mg/dl vs. ≈ 80 mg/dl wild type) and atherosclerotic lesions similar to those found in humans in both appearance and distribution [10]. The ApoE knockout has no sex bias and does not cause any reproductive issues allowing for safe and easy maintenance of the mouse colony. However, atherosclerosis is more severe in female mice [63]. The increase in total plasma cholesterol is unaffected by age or sex [55].

The apoE$^{-/-}$ mice used in this project were obtained from Jax Laboratory and have been backcrossed into a C57BL/6 genetic background. These mice spontaneously develop fatty streaks in the aortic sinus by 10-12 weeks of age. Lesion size increases with age and can become quite extensive [62,64].

3.1.2 ROSA26-FLOXSTOP-VEGF$_{164}$

The ROSA26-FLOXSTOP-VEGF$_{164}$ mice were obtained from the Andras Nagy lab (Lunenfeld-Tanenbaum Research Institute) [65]. These mice have our gene of interest, the mouse isoform VEGF$_{164}$, inserted into the ROSA26 locus and expressed under the ROSA26 endogenous promoter. The ROSA26 locus is commonly used as a site for genetic insertion because it is expressed in all cell

types and developmental stages, but the mRNA is not translated into a protein. This allows for the insertion of genes under a ubiquitous promoter without disrupting the expression of any existing proteins [66].

Upstream of the VEGF cDNA insertion, a transcription stop sequence flanked by LoxP sites has been inserted. This prevents transcription of the VEGF gene. The presence of a Cre recombinase is required to cleave the loxP sites and removes the transcriptional stop, allowing for the transcription and translation of the VEGF transgene [65].

3.1.3 Tg(Csf1r-cre/Esr1*)1Jwp/J

Macrophages are the predominant cell type within the atherosclerotic lesion. Our previous experiments have suggested that lesional macrophages are the major source of inflammation and hypoxia within the atherosclerotic plaque [37]. We expect to concentrate VEGF expression in atherosclerotic lesions by expressing VEGF specifically in macrophages. However, it should be noted that all macrophages will be affected.

In order to create a mouse that will express the VEGF transgene in a macrophage-specific and tamoxifen-inducible manner (**Figure 5**), mice carrying a Cre recombinase transgene with these properties were obtained from Jax Laboratory [67]. These mice express a modified Cre recombinase that is fused to two mutant murine estrogen receptors on each end. This modified Cre recombinase is expressed under the control of a macrophage-specific promoter

of colony-stimulating factor 1 receptor (CSF1R), a tyrosine kinase receptor essential in macrophage differentiation [68]. The mutated estrogen receptors do not bind estrogen but do bind the synthetic estrogen receptor ligand, 4-hydroxytamoxifen (OHT or tamoxifen). Mice are injected with tamoxifen, which is metabolized to OHT. When OHT/tamoxifen binds to the fusion construct, the recombinase relocates to the nucleus, where it is active [67]. In the absence of tamoxifen, inactive Cre recombinase is expressed in macrophages. In the presence of tamoxifen, it is activated and promotes the expression of VEGF.

3.1.4 Crossing Strategy to Obtain VEGF$^{tg/0}$CSF1R-iCRE$^{tg/0}$apoE$^{-/-}$ Experimental Mice

All studies involving mice were performed according to the guidelines and regulations of the Canadian Council on Animal care. All animal studies were pre-approved by McMaster University Animal Research Ethics Board. The genotype of all mice was verified before breeding or enrollment into the experiment (**Figure 6**). The following crossing strategy was utilized to obtain VEGF$^{tg/0}$CSF1R-iCRE$^{tg/0}$apoE$^{-/-}$ experimental mice and CSF1R-iCRE$^{tg/0}$apoE$^{-/-}$ and VEGF$^{tg/0}$apoE$^{-/-}$ controls (**Figure 4**).

ROSA26-FLOXSTOP-VEGF$_{164}$ double knock-in mice (VEGF$^{tg/tg}$) obtained from the Andras Nagy lab (Lunenfeld-Tanenbaum Research Institute, Toronto) were backcrossed into a C57BL/6J (JAX, USA) background five times [65]. ApoE$^{-/-}$ mice also have a C57BL/6J background. VEGF$^{tg/0}$ mice were paired with

apoE$^{-/-}$ to obtain VEGF$^{tg/0}$apoE$^{+/-}$ mice (50% of littermates). VEGF$^{tg/0}$apoE$^{+/-}$ progeny were crossed with genetically identical cousins to produce VEGF$^{tg/tg}$apoE$^{-/-}$ (6.25% of littermates). VEGF$^{tg/tg}$apoE$^{-/-}$ mice were crossed with genetically identical cousins to produce litters that were 100% VEGF$^{tg/tg}$apoE$^{-/-}$ mice (**Figure 4A**). The colony is maintained through cousin pairing.

Tg(Csf1r-cre/Esr1*)1Jwp/J single gene knock-in (CSF1R-iCRE$^{tg/0}$) were backcrossed into a C57BL/6J background ten times and then crossed with apoE$^{-/-}$ mice over three generations to obtain CSF1R-iCRE$^{tg/0}$apoE$^{-/-}$ mice (50% of littermates). The colony is maintained by pairing CSF1R-iCRE$^{tg/0}$apoE$^{-/-}$ with apoE$^{-/-}$ mice from a separate apoE$^{-/-}$ only colony (**Figure 4B**).

VEGF$^{tg/tg}$apoE$^{-/-}$ mice from the first colony were crossed with CSF1R-iCRE$^{tg/0}$apoE$^{-/-}$ mice from the second colony to create the experimental mice, VEGF$^{tg/0}$CSF1R-iCRE$^{tg/0}$apoE$^{-/-}$ mice (50% of littermates), and CRE negative controls, VEGF$^{tg/0}$apoE$^{-/-}$ mice (50% of littermates). The VEGF$^{tg/0}$CSF1R-iCRE$^{tg/0}$apoE$^{-/-}$ mice carry one copy of the floxed VEGF gene, one copy of the macrophage-specific inducible Cre recombinase gene and are double knockouts for apolipoprotein E. The colony is maintained by pairing mice from the first two colonies (**Figure 4C**). VEGF is only overexpressed after tamoxifen-induced activation of Cre recombinase removes the floxed transcriptional stop located upstream of the exogenous VEGF gene (**Figure 5**).

Figure 4: Breeding scheme to create VEGF$^{tg/0}$CSF1R-iCRE$^{tg/0}$apoE$^{-/-}$ mice. *(Created with BioRender)* **A.** VEGF$^{tg/tg}$ mice obtained from the Nagy Lab (Toronto, ON) contain cDNA encoding the VEGF-A$_{164}$ gene with a floxed transcriptional stop inserted in the ROSA26 locus. The transcriptional stop prevents the VEGF transgene from transcription under normal conditions. VEGF$^{tg/tg}$ mice were crossed into a C57BL/6J background and then crossed with apoE$^{-/-}$ mice to create VEGF$^{tg/tg}$apoE$^{-/-}$ mice. **B.** CSF1R-iCRE$^{tg/0}$ mice obtained from Jackson Laboratories contain a gene encoding tamoxifen-inducible Cre recombinase under the control of a macrophage-specific promoter. The Cre recombinase is transcribed and translated only in macrophages. The recombinase is localized to the cytoplasm and is therefore inactive under normal conditions. CSF1R-iCRE$^{tg/0}$ mice were backcrossed into a C57BL/6J background and then crossed with apoE$^{-/-}$ mice to create CSF1R-iCRE$^{tg/0}$apoE$^{-/-}$ mice. Some CSF1R-iCRE$^{tg/0}$apoE$^{-/-}$ mice were used as controls lacking the VEGF transgene. **C.** VEGF$^{tg/tg}$apoE$^{-/-}$ mice were crossed with CSF1R-iCRE$^{tg/0}$apoE$^{-/-}$ mice to create VEGF$^{tg/0}$CSF1R-iCRE$^{tg/0}$apoE$^{-/-}$ mice used in the experiments as well as VEGF$^{tg/0}$apoE$^{-/-}$ control mice lacking Cre recombinase.

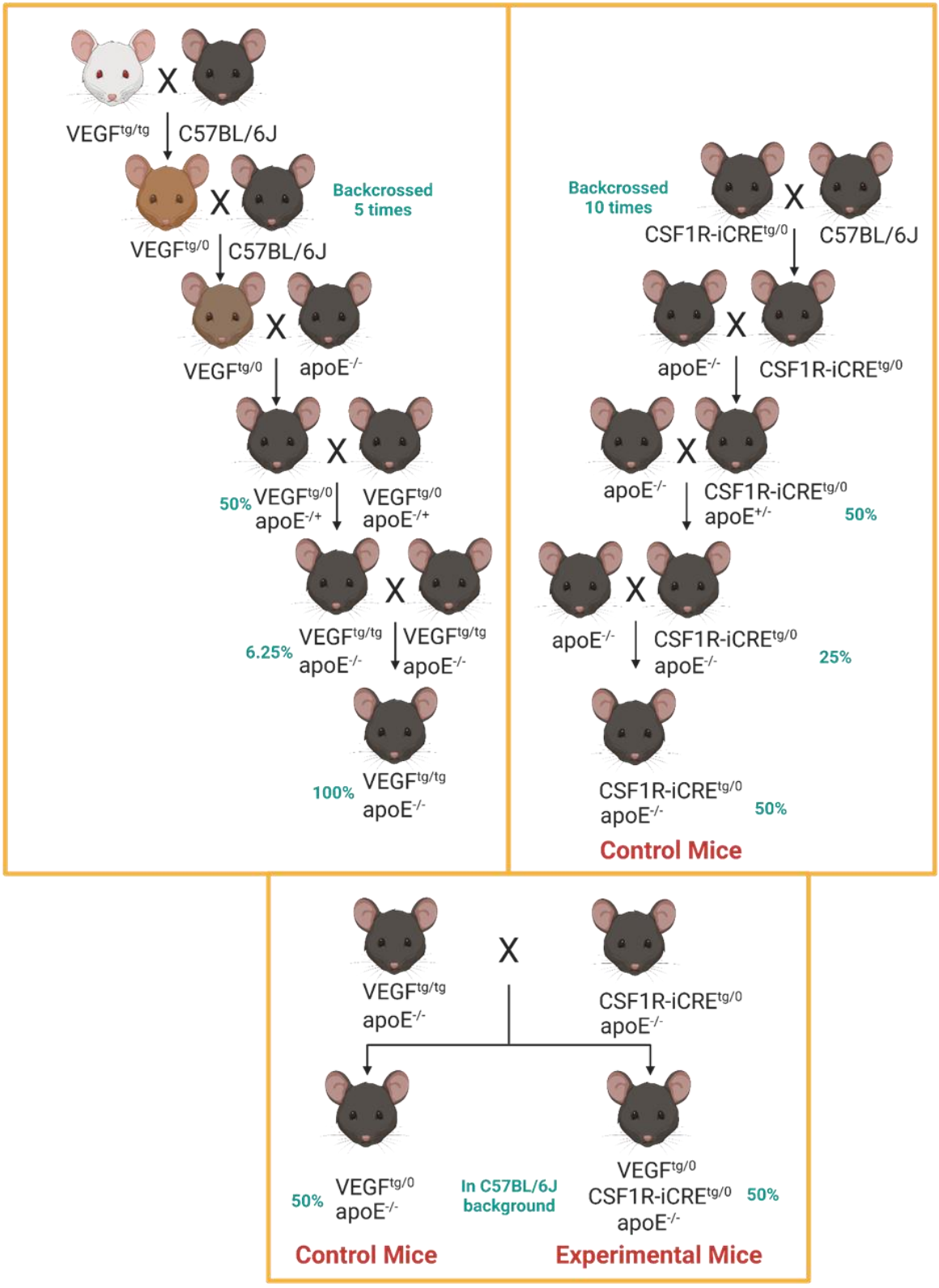
VEGF$^{tg/tg}$
C57BL/6J
Backcrossed 5 times
VEGF$^{tg/0}$
C57BL/6J
VEGF$^{tg/0}$
apoE$^{-/-}$
50%
VEGF$^{tg/0}$ apoE$^{-/+}$
VEGF$^{tg/0}$ apoE$^{-/+}$
6.25%
VEGF$^{tg/tg}$ apoE$^{-/-}$
VEGF$^{tg/tg}$ apoE$^{-/-}$
100%
VEGF$^{tg/tg}$ apoE$^{-/-}$
Backcrossed 10 times
CSF1R-iCRE$^{tg/0}$
C57BL/6J
apoE$^{-/-}$
CSF1R-iCRE$^{tg/0}$
apoE$^{-/-}$
CSF1R-iCRE$^{tg/0}$ apoE$^{+/-}$
50%
apoE$^{-/-}$
CSF1R-iCRE$^{tg/0}$ apoE$^{-/-}$
25%
CSF1R-iCRE$^{tg/0}$ apoE$^{-/-}$
50%
Control Mice
VEGF$^{tg/tg}$ apoE$^{-/-}$
CSF1R-iCRE$^{tg/0}$ apoE$^{-/-}$
50%
VEGF$^{tg/0}$ apoE$^{-/-}$
In C57BL/6J background
VEGF$^{tg/0}$ CSF1R-iCRE$^{tg/0}$ apoE$^{-/-}$
50%
Control Mice
Experimental Mice

Figure 5: Tamoxifen inducible macrophage-specific VEGF expression. *(Created with BioRender)* **A.** In non-macrophage cells of $VEGF^{tg/0}$CSF1R-$iCRE^{tg/0}apoE^{-/-}$ mice, the Cre recombinase is not transcribed and therefore, the VEGF transgene is not expressed. **B.** In macrophage cells, Cre recombinase is transcribed and translated, but the protein is not able to enter the nucleus to act as a DNA recombinase. **C.** When tamoxifen is injected into the mouse, it metabolizes to 4-hydroxytamoxifen (OHT). OHT binds to the mutated estrogen receptor domain of the Cre recombinase in the cytoplasm, promoting its translocation to the nucleus. Inside the nucleus, the Cre recombinase cleaves the loxP sites, removing the transcriptional stop upstream of the VEGF transgene, thus inducing the overexpression of the VEGF transgene.

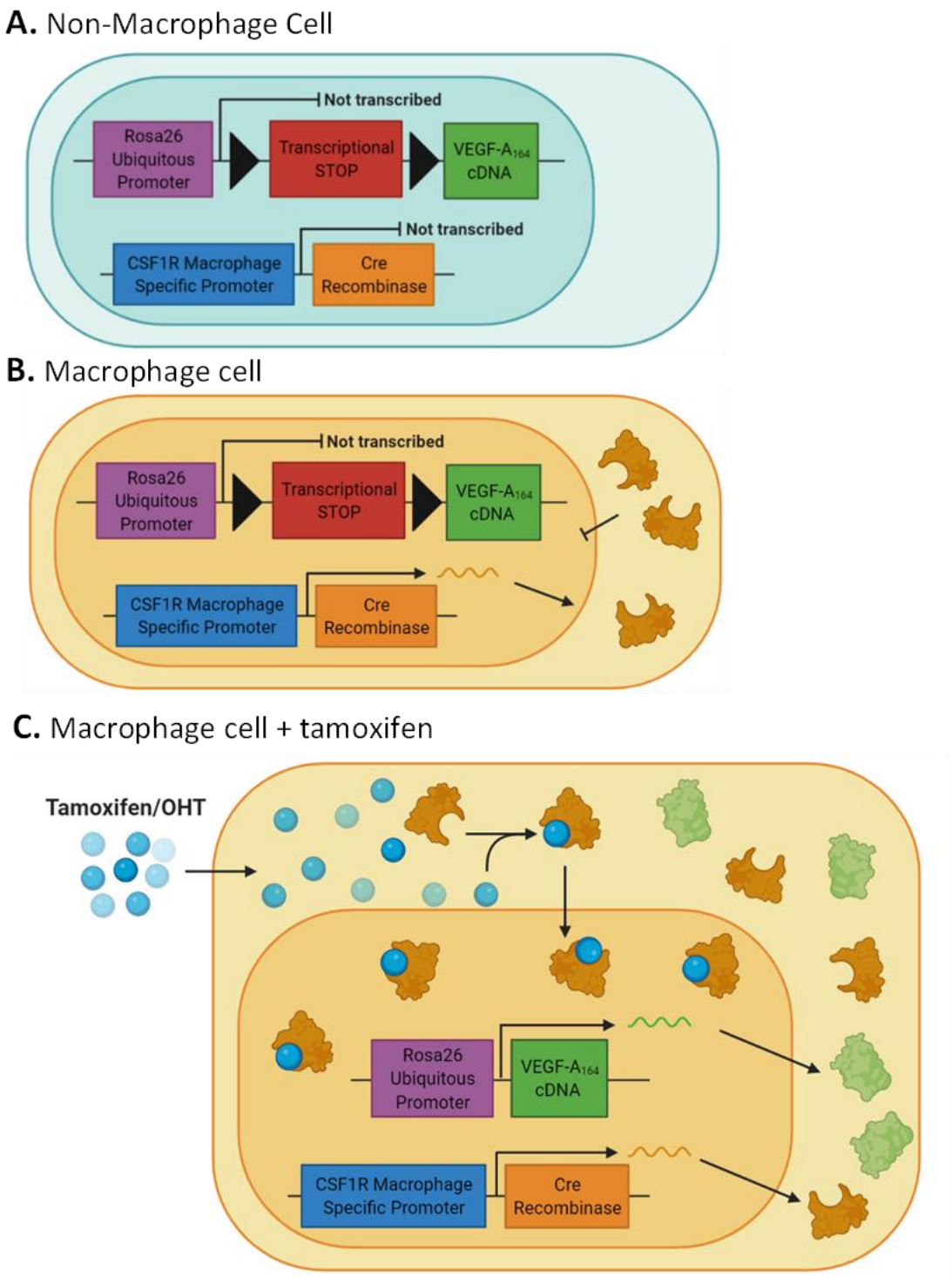
A. Non-Macrophage Cell
Not transcribed
Rosa26 Ubiquitous Promoter
Transcriptional STOP
VEGF-A164 cDNA
Not transcribed
CSF1R Macrophage Specific Promoter
Cre Recombinase
B. Macrophage cell
Not transcribed
Rosa26 Ubiquitous Promoter
Transcriptional STOP
VEGF-A164 cDNA
CSF1R Macrophage Specific Promoter
Cre Recombinase
C. Macrophage cell + tamoxifen
Tamoxifen/OHT
Rosa26 Ubiquitous Promoter
VEGF-A164 cDNA
CSF1R Macrophage Specific Promoter
Cre Recombinase

3.2 Genotyping

A 2-5mm tail sample was collected from each mouse and digested in lysis buffer containing proteinase K (PK) on a 60°C heat block for 90 minutes, followed by 10 minutes at 90°C to inactivate the PK. Samples were centrifuged at 6000 RPM for 30 seconds to remove cell debris. The DNA supernatant was stored at -20°C. The gene of interest was amplified using polymerase chain reaction (PCR). Specific primers and DNA were added to the Invitrogen Taq polymerase kit or the 1x GoTaq™ PCR Master Mix. Samples were processed in a PCR thermocycler based on specific conditions for each primer set. The PCR products and 100bp DNA ladder were run on a 1.2% agarose gel with ethidium bromide for 30 minutes. The gel was imaged under ultraviolet light. The PCR process was repeated to characterize each gene of interest. Mice with the desired genotype were selected and either paired as breeders or enrolled in an experimental study (**Figure 6**).

Figure 6: Genotyping CSF1R-iCRE, apoE, and VEGF. A. Primer sequences used for genotyping mice used in these experiments. Images of representative agarose gels illustrating **B.** CSF1R-iCRE genotyping using Invitrogen Taq polymerase kit. The presence of a band at 220bp indicates the knock-in of the iCre construct (lane 2), while the absence of a band at 220bp indicates WT (wildtype) mice (lane 1). **C.** ApoE genotyping using Promega GoTaq Master Mix. A band at 248bp indicates apoE knockout, while a band at 148bp indicates WT mice. Single apoE knockout mice have both bands (lanes 1, 2), double apoE knockout mice have only a 248bp band (lanes 3, 4), and WT mice have only a band at 148bp (lanes 5, 6). **D.** VEGF genotyping using Promega GoTaq Master Mix. A band at 300bp indicates VEGF knock-in, while a band at 600bp indicates WT mice. Mice with a single copy of VEGF have both bands (lanes 1, 2), WT mice have only a 600bp band (lanes 3, 4), and double VEGF knock-in mice have only a band at 300bp (lanes 5, 6).

A.

Gene	Forward Primer (5' → 3')	Reverse Primer (5' → 3')
CSF1R-iCRE	AGATGCCAGGACATCAGGAACCTG	ATCAGCCACACCAGACACAGAGATC
ApoE WT	GCCGCCCCGACTGCATCT	TGTGACTTGGGAGCTCTGCAGC
ApoE Knockout Mutant	GCCGCCCCGACTGCATCT	GCCTAGCCGAGGGAGAGCCG
ROSA26 WT	AAAGTCGCTCTGAGTTGTTAT	GGAGCGGGAGAAATGGATATG
ROSA26-FLOXSTOP-VEGF-A_{164} Transgene	AAAGTCGCTCTGAGTTGTTAT	GCGAAGAGTTTGTCCTCAACC

B.

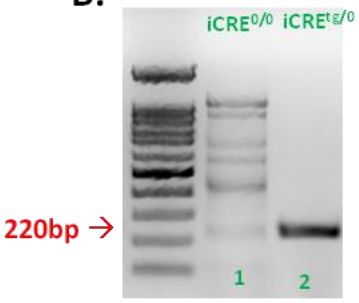

C.

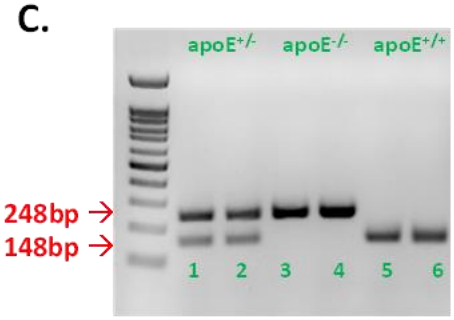

D.

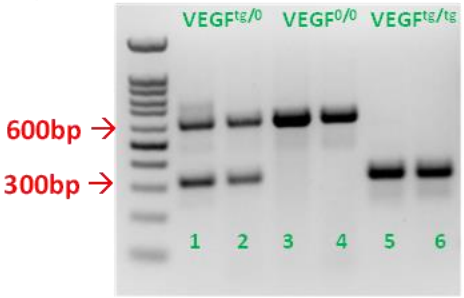

3.3. Induction of Hyperglycemia via Streptozotocin Injection

Streptozotocin (STZ) is a DNA alkylating agent that induces insulin-dependent DM through selective toxicity of pancreatic beta cells [69]. STZ was stabilized in a solution of 0.02M Citrate Buffer pH 4.5 at a concentration of 15mg/mL directly prior to injections. A low-dose regimen was utilized by administering STZ at a dose of 50mg/kg of body weight to each mouse through intraperitoneal (IP) injection for five consecutive days, followed by a week break and another round of five consecutive injections. STZ was administered to mice starting at five weeks of age. Citrate buffer was administered to normoglycemic controls following the same regimen. All injections were administered under anesthesia. Blood glucose was measured using a blood glucose monitor (OneTouch Verio Flex) through saphenous vein bleed before the STZ regimen and every three weeks following until sacrifice. A blood glucose level above 15mM after a 4-hour fast was used to confirm hyperglycemia. STZ-injected mice with blood glucose levels ≤ 15mM were eliminated from the study.

3.4. Induction of Cre via Tamoxifen Injection

Tamoxifen was injected into mice to induce Cre recombinase activity. Tamoxifen was dissolved and stabilized in a solution of ethanol and corn oil (90% corn oil) to a concentration of 22.54mg/mL. The solution was placed on a rocker at 37°C for 4 hours to dissolve completely and stored at 4°C for up to a week.

Mice were injected IP with tamoxifen for five consecutive days at a dose of 75mg/kg of body weight starting at either six weeks or ten weeks of age. Corn oil was administered to controls at six weeks of age for five consecutive days. All injections were administered under anesthesia.

3.5 Experiment Design

Two separate experimental designs have been implemented:

The objective of the first is to determine how long VEGF is overexpressed in macrophages after induction with tamoxifen and to examine any possible off-target effects in the liver (**Figure 7).**

The objective of the second is to examine the effects of VEGF overexpression at two different time points in the development and progression of atherosclerosis in normoglycemic and hyperglycemic mice (**Figure 8**).

The study required two separate experiments because the process of isolating peritoneal macrophages for collection induces a whole-body immune response that may affect the analysis of other organs/tissues and systems of the body.

3.5.1 Experiment 1

To examine the temporal and tissue specificity of VEGF overexpression, $VEGF^{tg/0}$CSF1R-$iCRE^{tg/0}apoE^{-/-}$ and $VEGF^{tg/0}apoE^{-/-}$ mice were enrolled.

VEGF$^{tg/0}$CSF1R-iCRE$^{tg/0}$apoE$^{-/-}$ mice received either tamoxifen or corn oil and VEGF$^{tg/0}$apoE$^{-/-}$ mice received tamoxifen at six weeks of age. Mice were sacrificed at three different time points: 1-week, 5-weeks and 9-weeks after the last tamoxifen injection. Both female and male mice were enrolled in the study, with a sample size of three in each unique experimental group. Intraperitoneal macrophages, spleen, liver, and heart were collected after sacrifice (**Figure 7**).

Figure 7: Experimental design to investigate temporal and tissue specificity of VEGF overexpression. *(Created with BioRender)* Six-week-old VEGF$^{tg/0}$CSF1R-iCRE$^{tg/0}$apoE$^{-/-}$ mice and VEGF$^{tg/0}$apoE$^{-/-}$ mice were injected with tamoxifen to investigate the specificity and other effects of Cre recombinase expression. A separate subset of six-week-old VEGF$^{tg/0}$CSF1R-iCRE$^{tg/0}$apoE$^{-/-}$ mice were injected with corn oil to control for the potential effects of tamoxifen. Mice from each group were sacrificed at 7, 11 and 15 weeks of age (corresponding to 1,5 and 9 weeks post tamoxifen injection) and peritoneal macrophages, blood, whole heart and aorta and liver were collected and processed for analysis. Both male and female mice will be enrolled in the study to account for sex differences. n=3 from each sex.

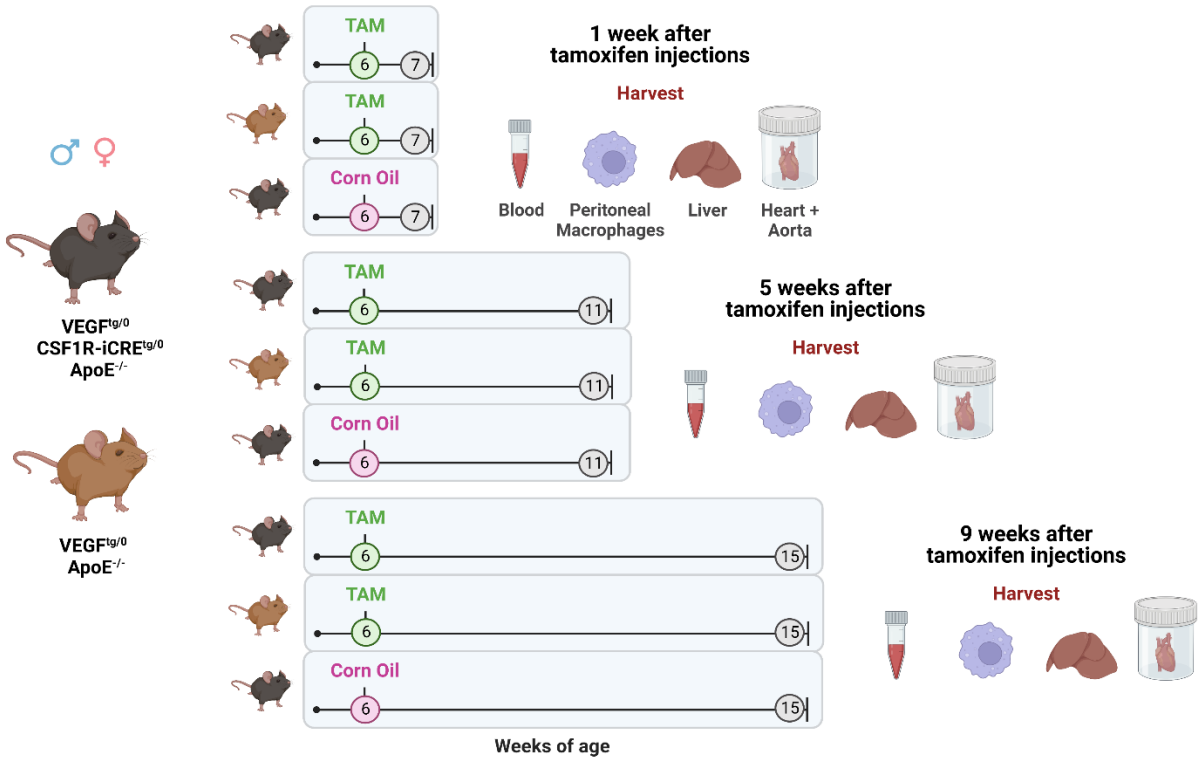
♂ ♀
VEGF^tg/0
CSF1R-iCRE^tg/0
ApoE^-/-
VEGF^tg/0
ApoE^-/-
TAM
Corn Oil
6
7
11
15
1 week after tamoxifen injections
Harvest
Blood
Peritoneal Macrophages
Liver
Heart + Aorta
5 weeks after tamoxifen injections
Harvest
9 weeks after tamoxifen injections
Harvest
Weeks of age

3.5.2 Experiment 2

To examine the effect of VEGF overexpression in atherosclerosis, both $VEGF^{tg/0}$CSF1R-$iCRE^{tg/0}apoE^{-/-}$ and CSF1R-$iCRE^{tg/0}apoE^{-/-}$ mice were enrolled. Three tamoxifen time points were used with $VEGF^{tg/0}$CSF1R-$iCRE^{tg/0}apoE^{-/-}$ mice: tamoxifen at six weeks of age, tamoxifen at ten weeks of age, and no-tamoxifen (corn oil) controls. $VEGF^{tg/0}$CSF1R-$iCRE^{tg/0}apoE^{-/-}$ mice were either maintained as normoglycemic (IP injections of citrate buffer) or subjected to STZ-induced hyperglycemia. Normoglycemic CSF1R-$iCRE^{tg/0}apoE^{-/-}$ mice were injected with tamoxifen at six weeks of age. Both female and male mice were used with a sample size of eight in each unique experimental group (**Figure 8**).

Figure 8: Experimental design to investigate the effect of VEGF overexpression on atherosclerosis. *(Created with BioRender)* Five-week-old male and female VEGF$^{tg/0}$CSF1R-iCRE$^{tg/0}$apoE$^{-/-}$ mice were injected with STZ to induce hyperglycemia or with citrate buffer as normoglycemic controls at 5 and 7 weeks of age. Subsets of mice were injected with tamoxifen (TAM) to induce VEGF transgene expression at 6 weeks of age or 10 weeks of age, controls will be injected with corn oil vehicle. A separate control group of CSF1R-iCRE$^{tg/0}$apoE$^{-/-}$ mice, which do not contain the VEGF transgene, were injected with tamoxifen at 6 weeks of age. All mice were harvested at 15 weeks of age. Hearts were embedded in paraffin, sectioned, and stained for quantification. Blood samples were taken at harvest and analyzed for cholesterol and triglyceride levels. n=8

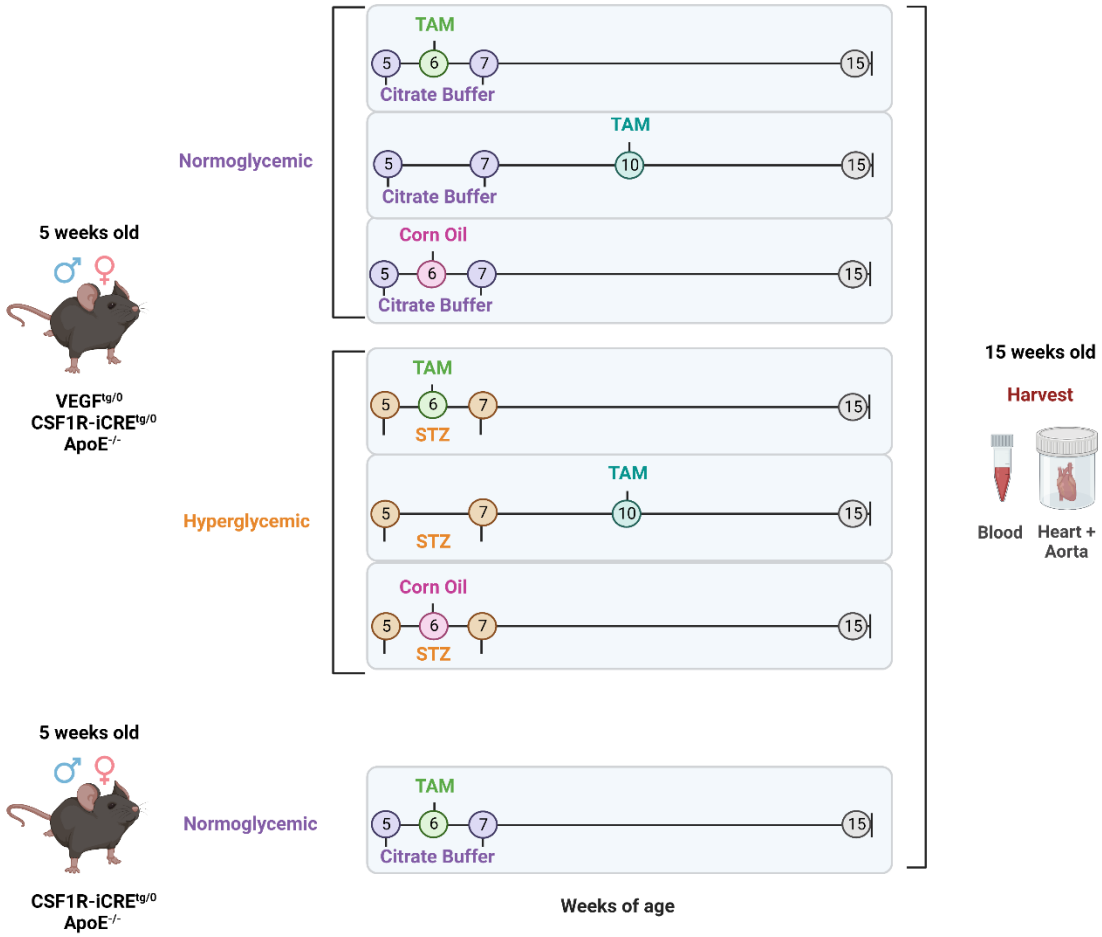
5 weeks old
VEGF tg/0
CSF1R-iCRE tg/0
ApoE -/-
Normoglycemic
TAM
Citrate Buffer
TAM
Citrate Buffer
Corn Oil
Citrate Buffer
Hyperglycemic
TAM
STZ
TAM
STZ
Corn Oil
STZ
5 weeks old
CSF1R-iCRE tg/0
ApoE -/-
Normoglycemic
TAM
Citrate Buffer
15 weeks old
Harvest
Blood
Heart + Aorta
Weeks of age

3.6 Peritoneal Macrophage and Heart Collection

Mice received 1mL of 10% thioglycollate via intraperitoneal injection while under anesthesia to elicit an inflammatory response and increase the number of peritoneal macrophages. Mice were monitored daily and given heat, gel or food on the cage bottom as required. Three days after the injection, a blood sample was taken via cardiac puncture and processed to isolate serum and plasma. Mice were then euthanized via cervical dislocation. The vasculature was flushed with 10mL of PBS via cardiac puncture. Mice were injected with sterile PBS+5mM EDTA into the peritoneum. The abdomen of the mice was massaged to dislodge cells, and the fluid was collected from the peritoneal cavity. Cells were centrifuged and plated with DMEM (10% FBS, 1% penicillin and streptomycin, 1% amino acids) in a six-well plate. After a two-hour incubation at 37°C, adherent macrophage cells were washed with sterile PBS and collected in protein lysis buffer or TRIzol to be stored at -80°C for downstream application.

3.7 Tissue Collection

Fasting blood glucose and total body weight was measured immediately prior to tissue collection. A blood sample was taken via cardiac puncture and processed to isolate serum and plasma. The mice were euthanized, and the vasculature was flushed with PBS. Perigonadal adipose, liver and pancreas were collected and weighed. Half of each tissue was snap-frozen in liquid nitrogen, and

the other half was stored in 10% buffered formalin. The left eye, lung, kidney, and muscle samples were collected and snap-frozen in liquid nitrogen. A formalin drip was used for flushing the remaining organs with formalin via cardiac puncture. The right eye, lung, kidney, and muscle, as well as the brain, heart, whole aorta, and small intestine, were preserved in 10% buffered formalin.

3.8 Serum and Plasma Isolation

Collected blood was divided into two tubes, one containing the anticoagulant EDTA and one empty 1.5mL Eppendorf tube. The EDTA tube was promptly placed on ice immediately following blood collection. The non-EDTA tube was left at room temperature to coagulate. Both tubes were centrifuged at 6000 RPM for 5 minutes at 4°C. Serum was collected as the supernatant of the non-EDTA tube. The supernatant from the EDTA tube was centrifuged again at 12000 RPM for 5 minutes at 4°C. The plasma supernatant was collected into a new tube. Samples were stored at -80°C for subsequent analysis.

3.9 Processing of Hearts for Aortic Sinus Staining

A minimum of one week after collection and storage in formalin, hearts were processed for embedding. The heart was separated from the descending aorta and sectioned transversely directly below the atriums. The base of the heart was processed and embedded in paraffin. Precision sectioning was used to

locate the aortic sinus by identification of the aortic valve leaflets, as previously described [70]. Serial sections of 5µm thickness were collected on ten microscope slides. Sections were placed on slides in a 50µm distance sequence such that each slide provided a representative sample of the aortic sinus for subsequent analyses. A total of 500-600µm of the aortic sinus was sectioned and collected.

3.10 Immunofluorescence Staining

Slides containing serial sections of the aortic sinus were deparaffinized with heat and then submerged in xylene and rehydrated with ethanol and water. Warm and pressurized antigen unmasking solution was used to unmask the target epitopes. A blocking solution containing goat serum was used to prevent off-target antibody binding. Primary antibodies specific to the proteins of interest were diluted in a solution of 90% PBS-Triton 0.05% and 10% goat serum. The primary antibody solution was applied onto the slides and incubated at 4°C overnight. Primary antibodies used for immunofluorescence staining were directed against VEGF (sc-7269; Santa Cruz Biotechnology Inc; 1:50 dilution), VEGFR2 (55B11; Cell Signaling; 1:200 dilution), HIF1-α (NB100-105; Novus Bio; 1:50 dilution), and van Wilbon factor (A0082; DAKO; 1:50 dilution). The next day, the primary antibodies were removed, and the slides were washed with PBS. The appropriate (anti-mouse or anti-rabbit) Alexa Flour™ 488 goat IgG (H+L) secondary antibody was diluted 1:250 in PBS and applied directly to the slides

and incubated at room temperature for two hours. Slides were washed with PBS, and DAPI (D1306; Invitrogen, 1:5000 dilution) was applied to stain the nuclei. Coverslips were mounted on the slides using Fluoromount. Slides were stored in the dark at 4°C and imaged using the Leica STELLARIS 5 confocal microscope with LAS X imaging software.

For quantification of VEGF, VEGFR2, HIF1- α, and CD68, the percentage of plaque area stained was determined using ImageJ to select the plaque area, convert the image to 32bit and adjust the threshold to measure only the areas positively stained.

The vasa vasorum was identified by staining aortic cross sections with an antibody against von Willebrand factor (vWF), a useful marker of endothelial cells. Microvessels were identified as positively stained rings of cells less than 100μm in diameter. The total number of microvessels counted per sample was divided by the number of sections analyzed.

For all immunofluorescence quantification, only sections containing all three leaflets, undamaged during the process, were used for quantification. In addition, the top and bottom sections were omitted for immunofluorescence quantification to avoid inconsistent staining.

3.11 Masson’s Trichrome Staining

Masson’s trichrome staining was performed as previously described [70]. Slides containing serial sections of the aortic sinus were deparaffinized with heat

and then submerged in xylene and rehydrated with ethanol and water. Slides were stained with Weigert's iron hematoxylin, Biebrich scarlet-acid fuchsin, phosphomolybdic-phosphotungstic acid solution, and aniline blue. Slides were then dehydrated with ethanol, cleared in xylene and mounted with a Xylene-based mounting medium. Masson's trichrome staining stains collagen fibres blue, nuclei black, and the muscle, cytoplasm and keratin red.

3.12 Western Blot

Cell or tissue lysates were heated at 90°C for 10 minutes and loaded into a 10% SDS-PAGE gel along with a 100Kb protein ladder. The separated proteins were transferred onto a nitrocellulose membrane for 1.5h at 4°C. The membrane was blocked with 5% skim milk for 45 minutes to reduce non-specific binding. The primary VEGF antibody (JH121, Invitrogen) was applied and incubated at 4°C overnight. The next day, the membranes were washed with 1% skim milk before the polyclonal goat anti-mouse immunoglobulins/HRP secondary antibody (P0447; DAKO) was applied and incubated at room temperature for one hour. The membranes were imaged using the ChemiDoc imager. The membrane was then blocked and stained with an antibody against β-actin (A5441; Sigma Aldrich) for 30 minutes at 4°C, and the polyclonal goat anti-mouse immunoglobulins/HRP secondary antibody (P0447; DAKO) for 30 minutes at room temperature. Bands were quantified using ImageJ densitometry.

Macrophage samples frozen in lysis buffer were thawed before use. Bromophenol blue dye and dithiothreitol were added to stabilize proteins, and 30µL of each sample was loaded into each well. Primary anti-VEGF antibody (1:100) and anti-mouse secondary antibody (1:1000) were used. VEGF monomer bands were measured at ~23kda. The same membrane was probed for β-actin (1:5000) and anti-mouse secondary (1:10000) as a loading control. β-actin bands were measured at ~42kda.

Approximately 95-100mg of frozen liver sample was weighed and homogenized in lysis buffer using a glass grinder. Bromophenol blue dye and dithiothreitol were added to stabilize proteins, and 5µL of each sample was loaded into each well. Two membranes were loaded identically. One membrane was incubated with primary anti-VEGF antibody (1:5000) and anti-mouse secondary antibody (1:5000). VEGF dimer bands were measured at ~46kda. The other membrane was probed for β-actin (1:50000) and anti-mouse secondary (1:10000). β-actin bands were measured at ~42kda.

3.13 Cholesterol and Triglycerides Assay

Cholesterol and triglycerides were measured in blood plasma samples collected from fasted mice at 15 weeks of age. Firstly, 5µL of the sample was loaded into the wells, and then 200µL of either Infinity™ Cholesterol or Triglycerides Liquid Stable Reagent was added. Plates were shaken at 400 RPM for 1 minute and incubated at 37°C for 20 minutes. The optical density of each

well was determined by a microplate reader set to 500nm and a correction wavelength of 660nm. The concentration of cholesterol and triglycerides was determined using a standard curve of known concentrations.

3.14 Statistical Analysis

Data were analyzed by one-way ANOVA followed by Bonferroni's post hoc test for multiple comparisons using GraphPad Prism (v9.4.1). All data are expressed as mean ± SEM. For all experiments, a p-value of 0.05 or less was considered statistically significant.

4. RESULTS

4.1 Assessment of VEGF Overexpression in the VEGF$^{tg/0}$CSF1R-iCRE$^{tg/0}$apoE$^{-/-}$ Mouse Model

To test the effectiveness of the tamoxifen-inducible macrophage-specific VEGF$^{tg/0}$CSF1R-iCRE$^{tg/0}$apoE$^{-/-}$ mouse model in overexpressing VEGF, six-week-old male and female VEGF$^{tg/0}$CSF1R-iCRE$^{tg/0}$apoE$^{-/-}$ mice were injected with tamoxifen or corn oil as vehicle control (**Figure 7**). As an additional control, VEGF$^{tg/0}$apoE$^{-/-}$ transgene control mice, lacking the inducible Cre recombinase construct, were also injected with tamoxifen. Thioglycollate-induced peritoneal macrophages were collected from the peritoneal cavity one, five, and nine weeks following the injections of tamoxifen or corn oil. Adherent macrophages were isolated via a two-hour cell culture incubation at 37°C and PBS wash. A sample of the liver was also collected at these time points to act as a control. Protein lysates were prepared from peritoneal macrophages and liver tissue samples. Total protein lysates were resolved by SDS-PAGE and immuno-probed for VEGF protein and β-actin as a loading control.

Quantification of VEGF protein expression in peritoneal macrophages collected from both male and female mice shows a significant increase in VEGF protein expression in peritoneal macrophages one week after tamoxifen treatment compared to both the corn oil and Cre controls (**Figure 9A**). No

discernable differences or trends of VEGF expression in peritoneal macrophages collected from males or females at five- or nine-weeks following tamoxifen treatment were noted (**Figure 9BC**).

Quantification of VEGF protein expression in the liver shows that $VEGF^{tg/0}apoE^{-/-}$ control mice expressed lower levels of VEGF than $VEGF^{tg/0}$CSF1R-$iCRE^{tg/0}apoE^{-/-}$ mice five weeks after tamoxifen or corn oil treatment (Figure 9E). A similar but not significant trend in VEGF protein expression can be seen in liver samples one- and nine- weeks after treatment (Figure 9DF).

Further experiments with increased sample size are required to better understand these results and fully validate this model.

Figure 9: VEGF protein expression in intraperitoneal macrophages and liver protein lysate collected from normoglycemic male and female mice combined. Western blot analysis of intraperitoneal macrophages and liver protein lysates from $VEGF^{tg/0}$CSF1R-$iCRE^{tg/0}apoE^{-/-}$ (CRE) and control $VEGF^{tg/0}apoE^{-/-}$ (No CRE) mice injected with tamoxifen (TAM), and CRE mice injected with corn oil (CO) collected 1, 5, and 9 weeks after injections. Quantification of VEGF protein expression controlled to β-actin protein levels in macrophages **A.** 1 week, **B.** 5 weeks, and **C.** 9 weeks after tamoxifen injections and in liver **D.** 1 week, **E.** 5 weeks, and **F.** 9 weeks after tamoxifen injections. VEGF and β-actin bands used for quantification in **G.** male and **H.** female mice. n= 2-6, mean ± SEM, *p < 0.05, **p < 0.01, ns = not significant

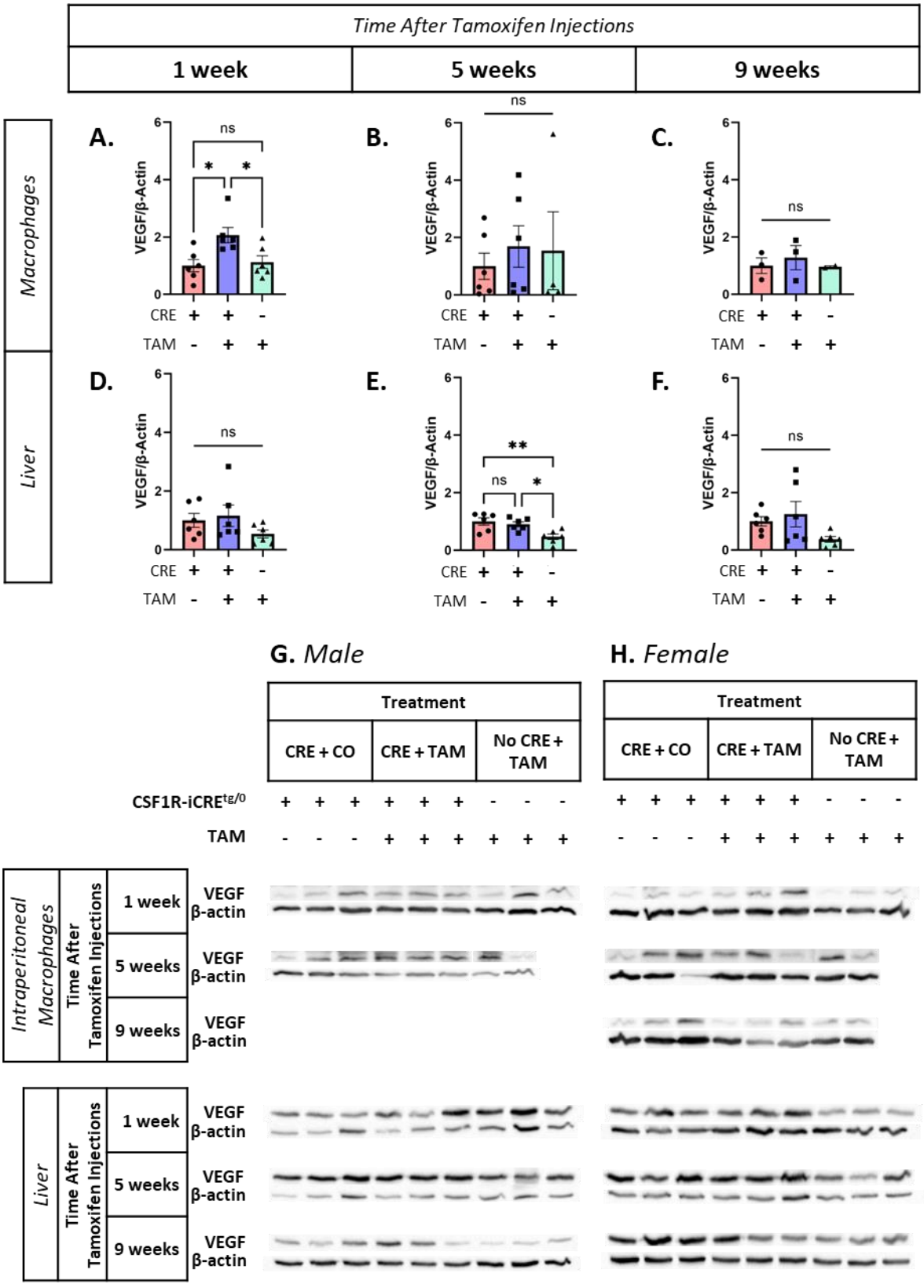
Time After Tamoxifen Injections
1 week
5 weeks
9 weeks
Macrophages
Liver
A.
B.
C.
D.
E.
F.
VEGF/β-Actin
ns
*
**
CRE + + -
TAM - + +
G. Male
H. Female
Treatment
CRE + CO
CRE + TAM
No CRE + TAM
CSF1R-iCRE^tg/0 + + + + + + - - -
TAM - - - + + + + + +
Intraperitoneal Macrophages
Time After Tamoxifen Injections
1 week
5 weeks
9 weeks
VEGF
β-actin
Liver

4.2 Metabolic Parameters, Organ Weights, and Blood Plasma Analysis

To study the effects of transient overexpression of VEGF on atherosclerosis in hyperglycemia, a second experiment was conducted using a separate group of mice.

Male and female VEGF$^{tg/0}$CSF1R-iCRE$^{tg/0}$apoE$^{-/-}$ and CSF1R-iCRE$^{tg/0}$apoE$^{-/-}$ mice were enrolled. Normoglycemic CSF1R-iCRE$^{tg/0}$apoE$^{-/-}$ mice were injected with tamoxifen at six weeks of age. Three tamoxifen time points were used with VEGF$^{tg/0}$CSF1R-iCRE$^{tg/0}$apoE$^{-/-}$ mice: tamoxifen at six weeks of age, tamoxifen at ten weeks of age, and no-tamoxifen (corn oil) controls. VEGF$^{tg/0}$CSF1R-iCRE$^{tg/0}$apoE$^{-/-}$ mice were either maintained as normoglycemic (IP injections of citrate buffer) or subjected to STZ-induced hyperglycemia.

Blood glucose was measured from enrollment at five weeks old to the endpoint at 15 weeks old to ensure STZ was effective in inducing hyperglycemia. Mice were considered hyperglycemic only if their fasting blood glucose was ≥ 15mM. Table 1 and Table 2 show that STZ was effective in inducing hyperglycemia in mice by eight weeks of age and was sustained until harvest at 15 weeks of age in both male and female mice. In female mice, no significant differences in blood glucose levels were noted among tamoxifen treatment groups. At the endpoint of 15 weeks of age, hyperglycemic male mice treated with tamoxifen at ten weeks of age had significantly higher blood glucose compared to age-matched hyperglycemic corn oil controls. In addition, body weight measurements show that by 15 weeks, almost all groups of hyperglycemic

mice were significantly lower in body weight compared to normoglycemic controls. However, female hyperglycemic mice injected with tamoxifen at six weeks old did not have a significant body weight difference from the normoglycemic control at 15 weeks of age.

To examine the effects of STZ and tamoxifen treatment on organs of the body beyond the aortic sinus, the liver, perigonadal adipose and pancreas were weighed and reported as a ratio relative to the body weight of each mouse. Tamoxifen treatment at six or ten weeks of age did not significantly impact the organ-to-body weight ratio of the liver, perigonadal adipose or pancreatic tissue (**Figure 10**). In both male and female hyperglycemic mice, liver weight-to-body weight ratios were increased (**Figure 10A**), and adipose weight-to-body weight ratios were decreased (**Figure 10B**) compared to normoglycemic controls of the same tamoxifen or corn oil treatment. Although STZ induces the apoptosis of pancreatic beta cells, pancreas weight to body weight ratios was unaffected in hyperglycemic groups compared to normoglycemic controls (**Figure 10C**).

Plasma cholesterol and triglycerides were measured to assess the potential dyslipidemic effects of the treatment groups. Tamoxifen treatments did not affect plasma cholesterol and triglycerides at six or ten weeks of age. Plasma cholesterol was significantly increased in both male and female hyperglycemic mice compared to normoglycemic controls (**Figure 11A**). Plasma triglycerides were unaffected by treatments (**Figure 11B**).

No significant differences in metabolic parameters, organs weights or plasma cholesterol and triglycerides between normoglycemic VEGF$^{tg/0}$CSF1R-iCRE$^{tg/0}$apoE$^{-/-}$ mice treated with tamoxifen at six weeks and CSF1R-iCRE$^{tg/0}$apoE$^{-/-}$ treatment matched control.

Figure 10: Organ to body weight ratios at 15 weeks of age. A. liver, **B.** perigonadal adipose, **C.** pancreas weight to body weight ratios of male and female normoglycemic (NG) and hyperglycemic (HG) VEGF$^{tg/0}$CSF1R-iCRE$^{tg/0}$apoE$^{-/-}$ mice at harvest (15 weeks of age). Tamoxifen (TAM) was injected at 6 or 10 weeks of age, as indicated. Mean ± SEM. *p < 0.05, **p < 0.01, ***p < 0.001, ****p < 0.0001, ns = not significant

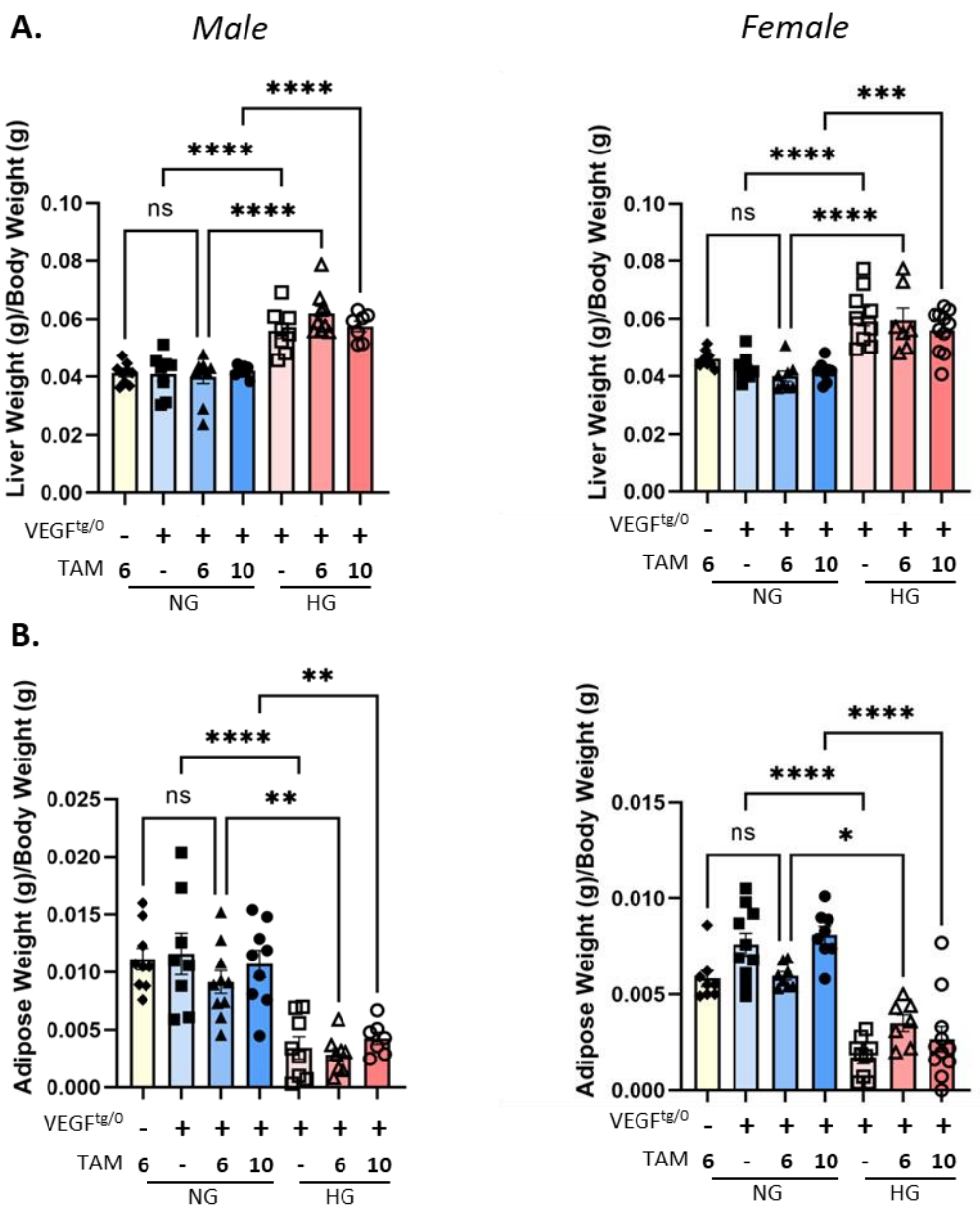
A.
Male
Female
Liver Weight (g)/Body Weight (g)
0.10
0.08
0.06
0.04
0.02
0.00
ns
****
****
***
VEGF tg/0 - + + + + + +
TAM 6 - 6 10 - 6 10
NG
HG
B.
Adipose Weight (g)/Body Weight (g)
0.025
0.020
0.015
0.010
0.005
0.000
**
****
ns
*

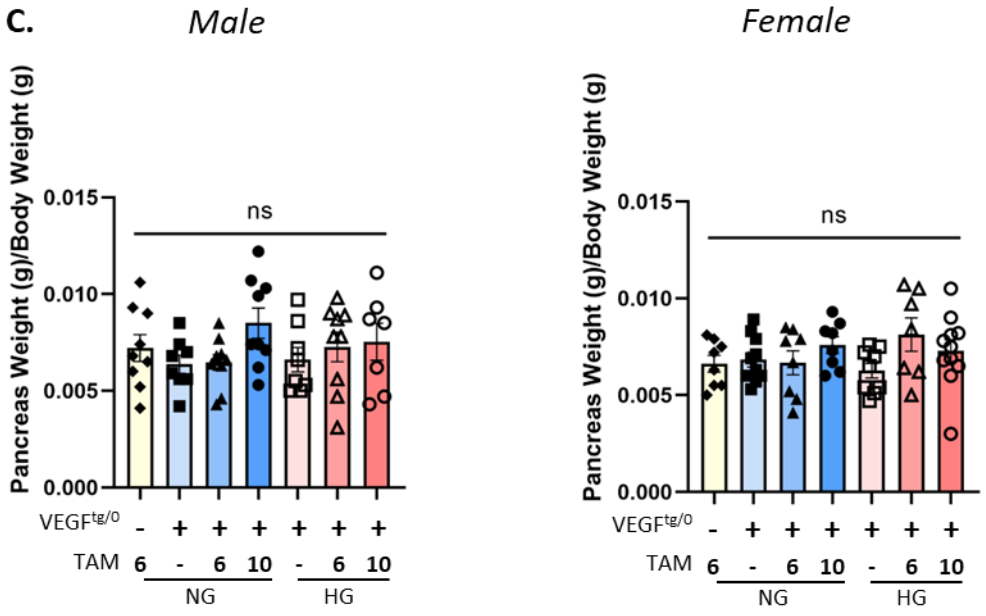
C.
Male
Female
Pancreas Weight (g)/Body Weight (g)
0.015
0.010
0.005
0.000
ns
VEGF tg/0
TAM
6
10
NG
HG

Figure 11: Fasting blood plasma analysis at 15 weeks of age. Quantification of **A.** plasma cholesterol and **B.** plasma triglycerides of male and female normoglycemic (NG) and hyperglycemic (HG) VEGF$^{tg/0}$CSF1R-iCRE$^{tg/0}$apoE$^{-/-}$ mice at harvest (15 weeks of age). Tamoxifen (TAM) was injected at 6 or 10 weeks of age, as indicated. Mean ± SEM. *p < 0.05, **p < 0.01, ***p < 0.001, ****p < 0.0001, ns = not significant

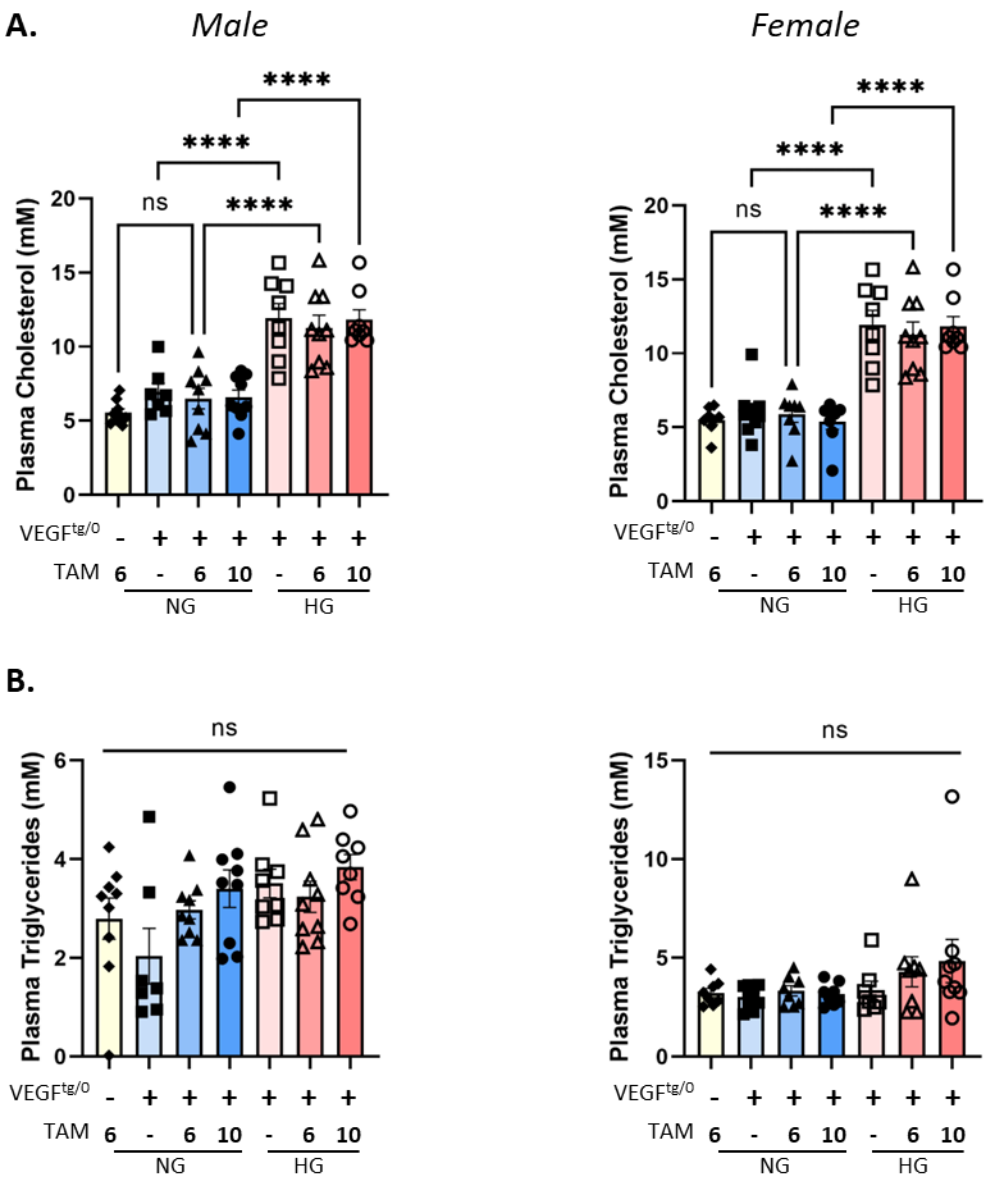
A.
Male
Female
Plasma Cholesterol (mM)
ns
****
****
****
VEGF tg/0
TAM
NG
HG
B.
Plasma Triglycerides (mM)
ns

Males								
Treatment	**Parameters**	***Age***						
		5 weeks	**8 weeks**		**11 weeks**		**15 weeks**	
		NG	**NG**	**HG**	**NG**	**HG**	**NG**	**HG**
Control	**Blood Glucose (mM)**	11.2 ± 1.6	10.6 ± 0.5	20.8 ± 2.0****	9.8 ± 0.7	27.2 ± 2.4****	8.9 ± 0.6	23.8 ± 2.0****
	Body Weight (g)	17.7 ± 1.0	23.3 ± 0.9	21.8 ± 1.1	26.1 ± 0.8	22.0 ± 1.0*	28.1 ± 0.8	22.8 ± 1.1**
	n	3	8	8	8	8	8	8
Tam 6 Weeks	**Blood Glucose (mM)**	10.2 ± 0.5	8.8 ± 0.7	21.3 ± 1.6****	11.0 ± 0.6	28.8 ± 1.8****	10.7 ± 0.4	27.3 ± 2.1****
	Body Weight (g)	18.9 ± 0.5	23.2 ± 0.6	20.3 ± 0.2	25.5 ± 0.9	22.8 ± 0.6	27.1 ± 0.8	23.4 ± 0.7*
	n	18	10	9	10	8	10	9
Tam 10 weeks	**Blood Glucose (mM)**	9.8 ± 0.4	10.7 ± 0.5	21.4 ± 1.7****	9.4 ± 0.5	26.2 ± 2.4****	9.7 ± 0.8	30.3 ± 1.7****,#
	Body Weight (g)	21.5 ± 1.0	26.1 ± 0.7	19.3 ± 0.8****	28.2 ± 0.6	22.8 ± 1.4**	28.7 ± 0.6	21.6 ± 0.8****
	n	11	9	8	9	7	9	8
		NG	**NG**	**NG No VEGF**	**NG**	**NG No VEGF**	**NG**	**NG No VEGF**
Tam 6 Weeks	**Blood Glucose (mM)**	10.2 ± 0.5	8.8 ± 0.7	8.5 ± 0.4	11.0 ± 0.6	10.6 ± 0.9	10.7 ± 0.4	9.4 ± 0.4
	Body Weight (g)	18.9 ± 0.5	23.2 ± 0.6	20.1 ± 1.0	25.5 ± 0.9	22.5 ± 1.2	27.1 ± 0.8	24.4 ± 1.3
	n	18	10	9	10	9	10	9

Table 1: Metabolic parameters for <u>male</u> mice. Ages and n values are indicated, mean ± SEM. VEGF$^{tg/0}$CSF1R-iCRE$^{tg/0}$apoE$^{-/-}$ mice unless otherwise indicated. *p < 0.05, **p < 0.01, ***p < 0.001, ****p < 0.0001 relative to age-matched NG controls, #p < 0.05 relative to age-matched corn oil control, NG = normoglycemic, HG = hyperglycemic, NG No VEGF = Normoglycemic CSF1R-iCRE$^{tg/0}$apoE$^{-/-}$ mice

Females								
Treatment	**Parameters**	*Age*						
		5 weeks	**8 weeks**		**11 weeks**		**15 weeks**	
		NG	**NG**	**HG**	**NG**	**HG**	**NG**	**HG**
Control	**Blood Glucose (mM)**	10.0 ± 0.3	9.2 ± 0.4	17.7 ± 1.0****	9.2 ± 0.5	25.2 ± 1.8****	9.2 ± 0.5	25.5 ± 2.4****
	Body Weight (g)	15.4 ± 0.7	18.8 ± 0.3	15.5 ± 0.4***	20.3 ± 0.4	17.8 ± 0.7	21.7 ± 0.5	18.0 ± 0.8**
	n	5	10	9	10	9	10	9
Tam 6 Weeks	**Blood Glucose (mM)**	9.7 ± 0.7	8.9 ± 0.3	19.2 ± 2.5****	9.3 ± 0.5	27.7 ± 1.8****	9.1 ± 0.5	26.0 ± 3.4****
	Body Weight (g)	15.8 ± 0.5	16.8 ± 0.3	16.8 ± 1.1	18.5 ± 0.4	18.5 ± 1.3	19.0 ± 0.4	19.7 ± 1.4
	n	11	8	7	8	7	8	7
Tam 10 weeks	**Blood Glucose (mM)**	9.6 ± 0.3	10.3 ± 0.4	16.3 ± 1.2**	10.1 ± 0.4	24.4 ± 1.3****	8.9 ± 0.6	27.3± 2.0****
	Body Weight (g)	16.2 ± .0.5	18.5 ± 0.5	15.3 ± 0.3***	20.8 ± 0.4	16.8 ± 0.4***	21.5 ± 0.5	16.8 ± 0.5***
	n	14	8	11	8	11	8	11
		NG	**NG**	**NG No VEGF**	**NG**	**NG No VEGF**	**NG**	**NG No VEGF**
Tam 6 Weeks	**Blood Glucose (mM)**	9.7 ± 0.7	8.9 ± 0.3	8.8 ± 0.5	9.3 ± 0.5	9.5 ± 0.4	9.1 ± 0.5	10.2 ± 0.3
	Body Weight (g)	15.8 ± 0.5	16.8 ± 0.3	17.1 ± 0.8	18.5 ± 0.4	18.9 ± 0.9	19.0 ± 0.4	19.5 ± 0.9
	n	11	8	8	8	8	8	8

Table 2: Metabolic parameters for <u>female</u> mice. Ages and n values are indicated, mean ± SEM. $VEGF^{tg/0}$CSF1R-$iCRE^{tg/0}apoE^{-/-}$ mice unless otherwise indicated. *p < 0.05, **p < 0.01, ***p < 0.001, ****p < 0.0001 relative to age-matched NG controls, NG = normoglycemic, HG = hyperglycemic, NG No VEGF = Normoglycemic CSF1R-$iCRE^{tg/0}apoE^{-/-}$ mice

4.3 Analysis of Atherosclerotic Plaques of Macrophage-Specific Inducible VEGF Mice at 15 Weeks of Age

Plaque volume within the aortic sinus of normoglycemic and hyperglycemic male and female $VEGF^{tg/0}CSF1R\text{-}iCRE^{tg/0}apoE^{-/-}$ mice was analysed, as previously described [70]. No significant differences were observed in any of the experimental and control groups of male mice (**Figure 12A**). In general, plaques were significantly smaller in the male mice compared to age-matched female mice, as previously observed [63].

In female mice, plaque volume was significantly increased in hyperglycemic corn oil controls compared to normoglycemic corn oil controls (**Figure 12B**). Tamoxifen injection had no significant effect on plaque volume in normoglycemic mice. Plaque volume was significantly decreased in hyperglycemic female mice administered tamoxifen at six weeks old compared to the hyperglycemic corn oil controls. A similar (non-significant) trend was observed in normoglycemic and hyperglycemic groups of male mice (**Figure 12A**).

Because significant effects on atherosclerotic plaque volume were observed in female, but not male mice, immunofluorescent staining of components of the hypoxia-mediated angiogenesis pathway (HIF-1α, VEGF, VEGFR2, and vasa vasorum density) was performed on only female mice due to time constraints.

In order to assess hypoxia in the artery wall, HIF-1α was assessed by immunofluorescent staining (**Figure 13**). Analysis of HIF-1α expression within the aortic plaques of female mice showed significant differences between normoglycemic and hyperglycemic groups and between tamoxifen treatments. Within the normoglycemic groups, a significant increase in HIF-1α was observed in the mice treated with tamoxifen at six weeks of age compared to corn oil controls. Within the hyperglycemic groups, mice treated with tamoxifen at six weeks of age had significantly elevated levels of HIF-1α compared to tamoxifen treatment at ten weeks of age. In addition, hyperglycemic mice injected with tamoxifen at ten weeks of age had higher HIF-1α expression within the plaques compared to normoglycemic controls administered the same tamoxifen treatment.

Analysis of VEGF and VEGFR2 expression within the aortic plaques at harvest (15 weeks of age) showed no significant differences in VEGF (**Figure 14**) or VEGFR2 (**Figure 15**) expression between tamoxifen treatment or glycemic groups. Analysis of vasa vasorum density also yielded no significant differences (**Figure 16**).

No significant differences in male and female plaque volume, female VEGF and HIF-1α staining or vasa vasorum density between normoglycemic $VEGF^{tg/0}$CSF1R-$iCRE^{tg/0}apoE^{-/-}$ mice treated with tamoxifen at six weeks and CSF1R-$iCRE^{tg/0}apoE^{-/-}$ treatment matched controls **(Figure 12-16).**

Figure 12: Atherosclerotic plaque quantification at 15 weeks of age.

Quantification of plaque volume in **A.** male and **B.** female normoglycemic (NG) and hyperglycemic (HG) VEGF$^{tg/0}$CSF1R-iCRE$^{tg/0}$apoE$^{-/-}$ mice at harvest (15 weeks of age). Tamoxifen (TAM) was injected at 6 or 10 weeks of age, as indicated. Representative images of Masson's Trichrome stained aortic sinus sections are shown. n=7-11 mice per group, mean ± SEM, *$p < 0.05$, **$p < 0.01$, ns = not significant

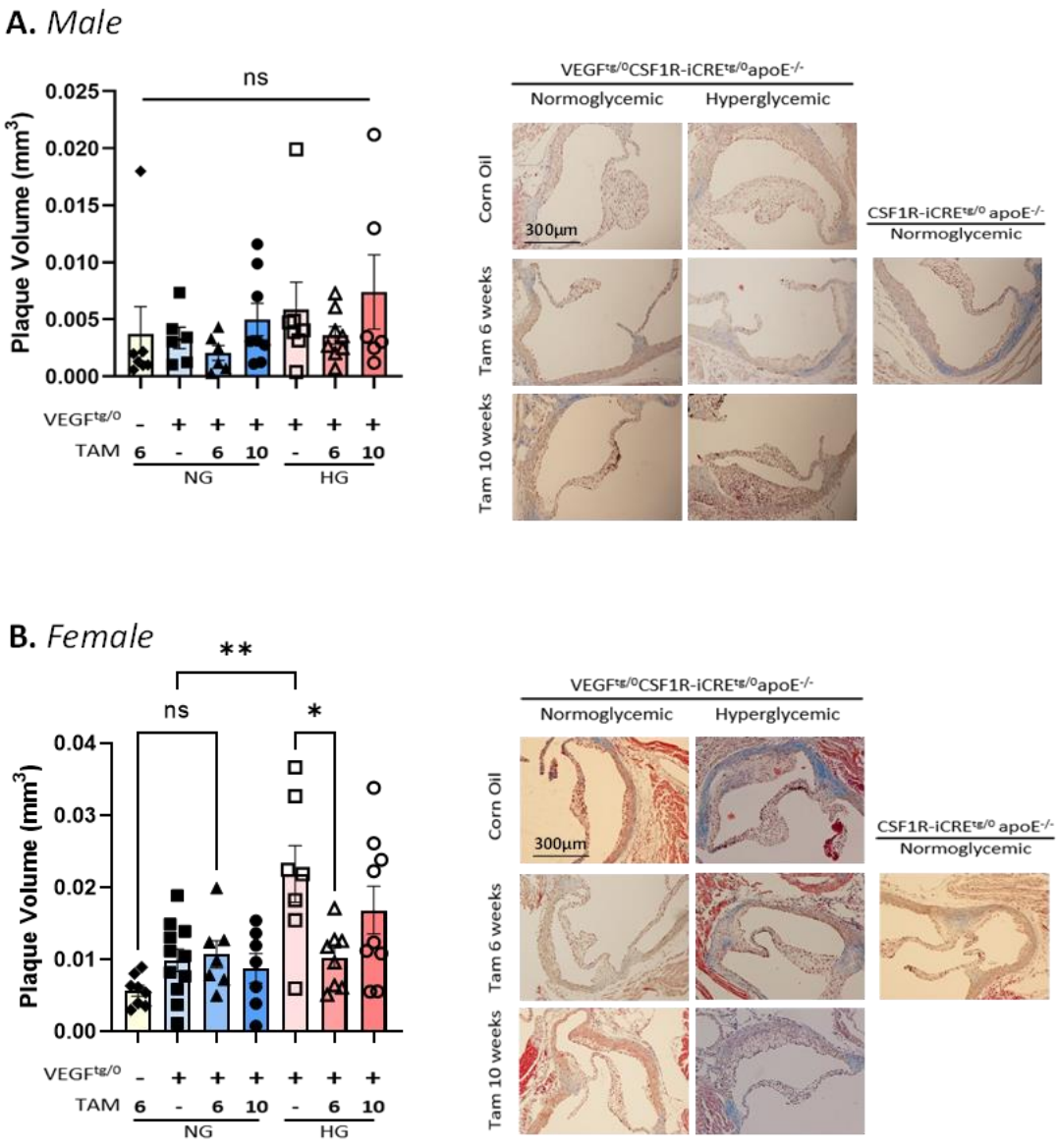
A. Male
ns
Plaque Volume (mm3)
0.025
0.020
0.015
0.010
0.005
0.000
VEGFtg/0 - + + + + + +
TAM 6 - 6 10 - 6 10
NG
HG
VEGFtg/0CSF1R-iCREtg/0apoE-/-
Normoglycemic
Hyperglycemic
Corn Oil
300µm
Tam 6 weeks
Tam 10 weeks
CSF1R-iCREtg/0 apoE-/-
Normoglycemic
B. Female
**
ns
*
Plaque Volume (mm3)
0.04
0.03
0.02
0.01
0.00
VEGFtg/0 - + + + + + +
TAM 6 - 6 10 - 6 10
NG
HG
VEGFtg/0CSF1R-iCREtg/0apoE-/-
Normoglycemic
Hyperglycemic
Corn Oil
300µm
Tam 6 weeks
Tam 10 weeks
CSF1R-iCREtg/0 apoE-/-
Normoglycemic

Figure 13: HIF-1α expression in atherosclerotic plaque of female mice at 15 weeks of age. Quantification of HIF-1α immunofluorescence staining within plaques of female normoglycemic (NG) and hyperglycemic (HG) VEGF$^{tg/0}$CSF1R-iCRE$^{tg/0}$apoE$^{-/-}$ mice at harvest (15 weeks of age). Tamoxifen (TAM) was injected at 6 or 10 weeks of age, as indicated. Representative images of HIF-1α stained aortic sinus sections and IgG anti-mouse non-specific immunofluorescent staining control. n=6-8 mice per group, mean ± SEM, *p < 0.05, ns = not significant

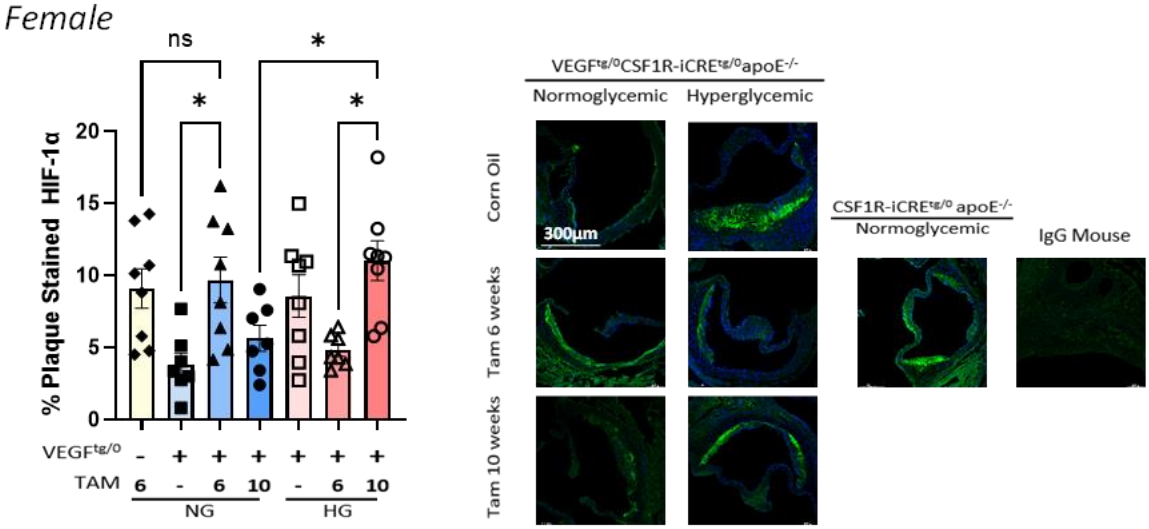
Female
ns
*
*
*
% Plaque Stained HIF-1α
20
15
10
5
0
VEGFtg/0 - + + + + + +
TAM 6 - 6 10 - 6 10
NG
HG
VEGFtg/0CSF1R-iCREtg/0apoE-/-
Normoglycemic
Hyperglycemic
Corn Oil
Tam 6 weeks
Tam 10 weeks
300µm
CSF1R-iCREtg/0 apoE-/-
Normoglycemic
IgG Mouse

Figure 14: VEGF expression in atherosclerotic plaque of female mice at 15 weeks of age. Quantification of VEGF immunofluorescence staining within plaques of female normoglycemic (NG) and hyperglycemic (HG) $VEGF^{tg/0}CSF1R\text{-}iCRE^{tg/0}apoE^{-/-}$ mice at harvest (15 weeks of age). Tamoxifen (TAM) was injected at 6 or 10 weeks of age, as indicated. Representative images of VEGF stained aortic sinus sections and IgG anti-mouse non-specific immunofluorescent staining control. n=6-8 mice per group, mean ± SEM, ns = not significant

Female

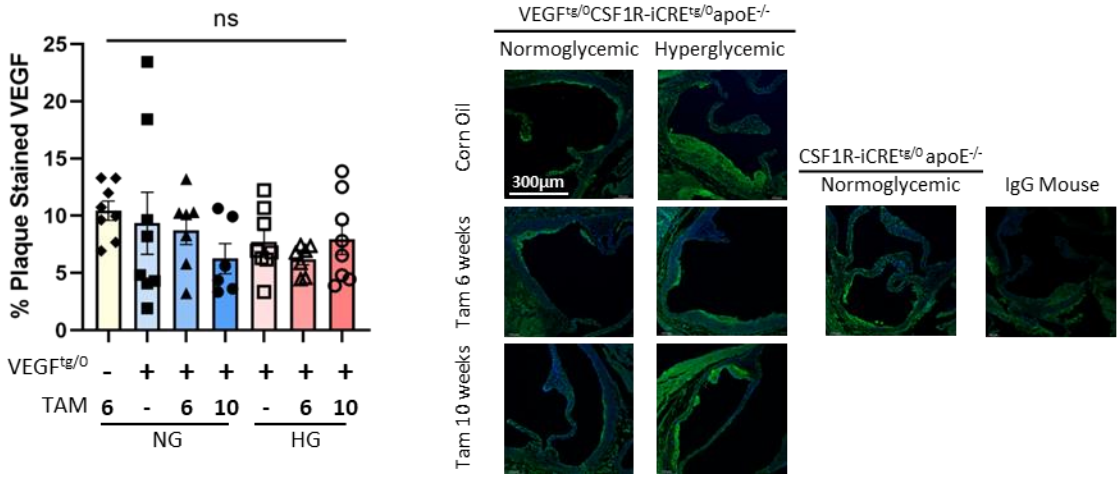
ns
% Plaque Stained VEGF
25
20
15
10
5
0
VEGF$^{tg/0}$ - + + + + + +
TAM 6 - 6 10 - 6 10
NG
HG
VEGF$^{tg/0}$CSF1R-iCRE$^{tg/0}$apoE$^{-/-}$
Normoglycemic
Hyperglycemic
Corn Oil
Tam 6 weeks
Tam 10 weeks
300µm
CSF1R-iCRE$^{tg/0}$ apoE$^{-/-}$
Normoglycemic
IgG Mouse

Figure 15: VEGFR2 expression in atherosclerotic plaque of female mice at 15 weeks of age. Quantification of VEGFR2 immunofluorescence staining within plaques of female normoglycemic (NG) and hyperglycemic (HG) $VEGF^{tg/0}CSF1R\text{-}iCRE^{tg/0}apoE^{-/-}$ mice at harvest (15 weeks of age). Representative images of VEGFR2 stained aortic sinus sections and IgG anti-rabbit non-specific immunofluorescent staining control. n=7-8 mice per group, mean ± SEM, ns = not significant

Female

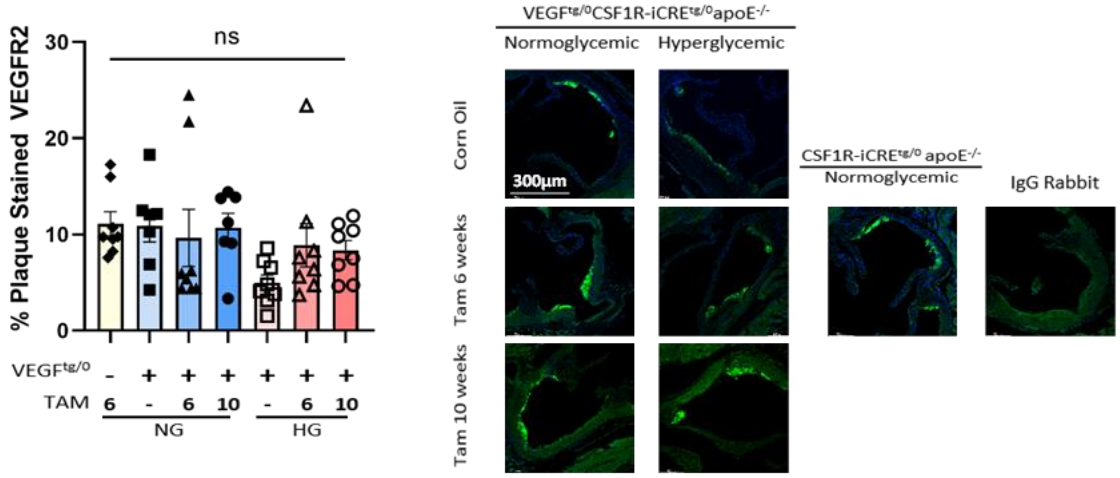
% Plaque Stained VEGFR2
ns
30
20
10
0
VEGF tg/0 - + + + + + +
TAM 6 - 6 10 - 6 10
NG
HG
VEGFtg/0CSF1R-iCREtg/0apoE-/-
Normoglycemic
Hyperglycemic
Corn Oil
Tam 6 weeks
Tam 10 weeks
300µm
CSF1R-iCREtg/0 apoE-/-
Normoglycemic
IgG Rabbit

Figure 16: Vasa vasorum density in the aortic sinus of female mice at 15 weeks of age. A. Quantification of vasa vasorum density by immunofluorescence staining of aortic sinus sections from female normoglycemic (NG) and hyperglycemic (HG) VEGF$^{tg/0}$CSF1R-iCRE$^{tg/0}$apoE$^{-/-}$ mice at harvest (15 weeks of age). Tamoxifen (TAM) was injected at 6 or 10 weeks of age, as indicated. Representative images of **B.** low and **C.** high vasa vasorum density. Arrows indicate positively stained microvessels. n=5-10 mice per group, ns = not significant

Female

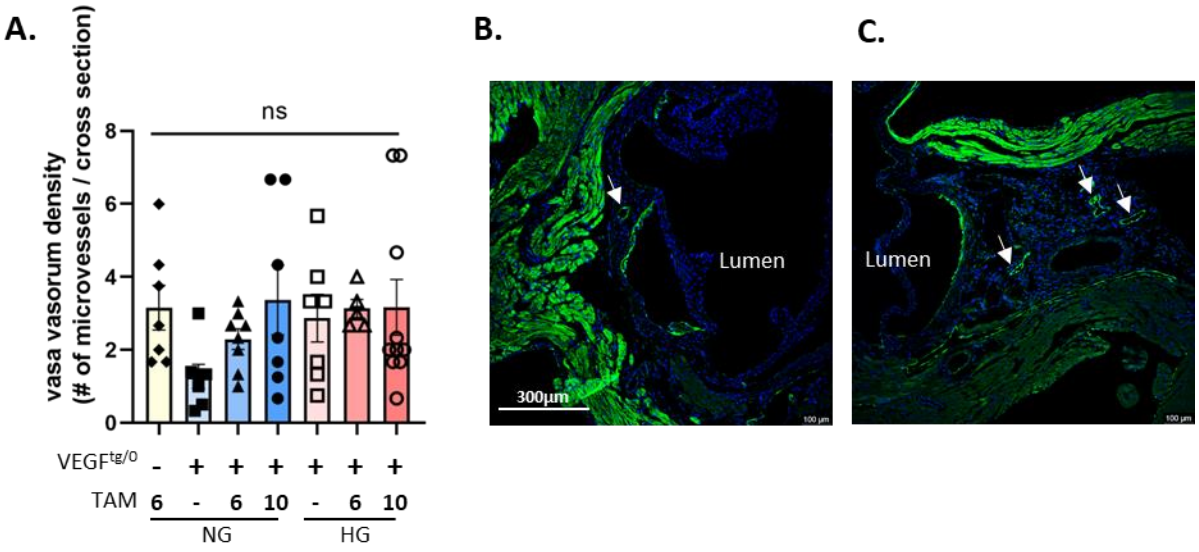
A.
B.
C.
ns
vasa vasorum density
(# of microvessels / cross section)
8
6
4
2
0
VEGF$^{tg/0}$ - + + + + + +
TAM 6 - 6 10 - 6 10
NG
HG
Lumen
300µm
Lumen

4.4 Atherosclerotic Plaque Volume in the Aortic Sinus One and Five Weeks After Tamoxifen Injections

During peritoneal macrophage and liver collection, the heart and aorta were also collected and processed for atherosclerotic plaque analysis. This allows us to better understand the effects of VEGF overexpression at six weeks of age in normoglycemic male and female mice by analyzing atherosclerotic plaque progression at two earlier endpoints.

However, likely due to the very small sample size, analysis of plaque volume within the aortic sinus of male and female $VEGF^{tg/0}$CSF1R-$iCRE^{tg/0}apoE^{-/-}$ mice collected one or five weeks after tamoxifen or corn oil injections yielded no significant results (**Figure 17**).

Figure 17: Atherosclerotic plaque quantification one or five weeks after tamoxifen treatment. Quantification of plaque volume in **A**. male and **B.** female from $VEGF^{tg/0}CSF1R\text{-}iCRE^{tg/0}apoE^{-/-}$ mice injected with tamoxifen (TAM) or corn oil (CO) collected 1 or 5 weeks after injections. **C.** Representative images of Masson's Trichrome stained aortic sinus sections. n=3 mice per group, mean ± SEM, ns = not significant

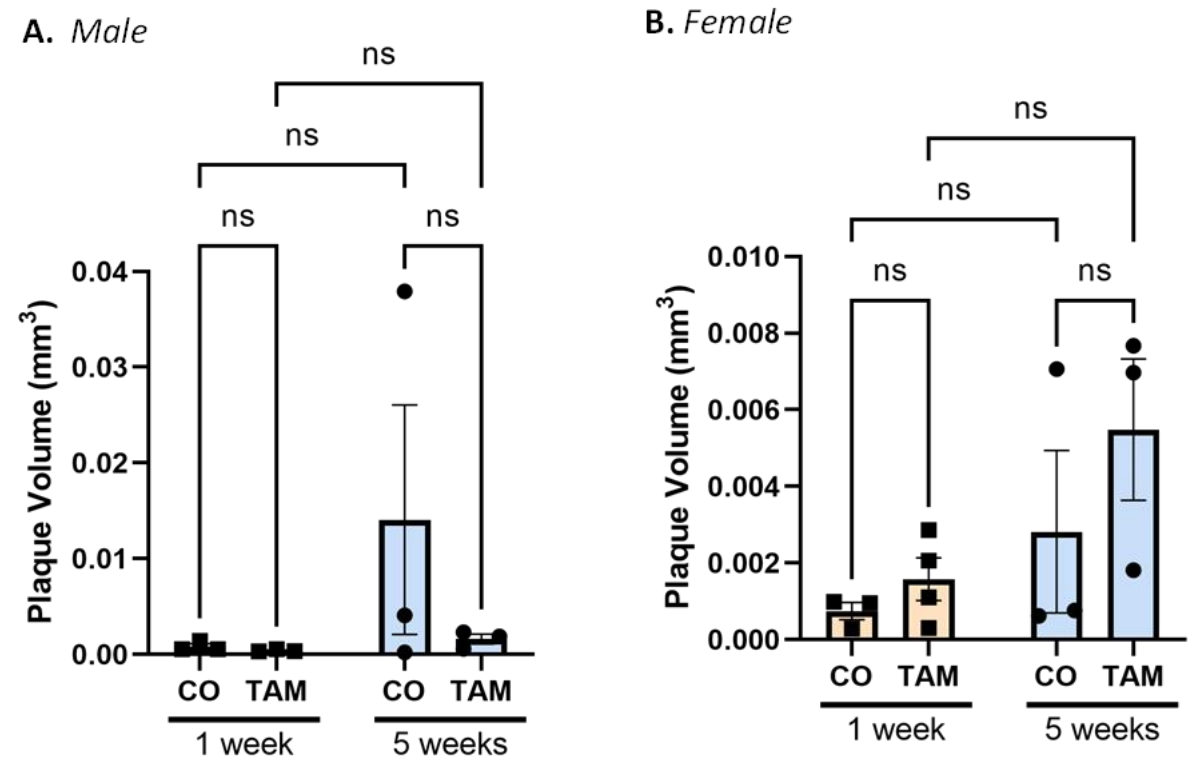
A. Male
B. Female
ns
Plaque Volume (mm3)
0.04
0.03
0.02
0.01
0.00
0.010
0.008
0.006
0.004
0.002
0.000
CO
TAM
1 week
5 weeks
C.
Male
Female
200µm

5. DISCUSSION

A recent global analysis of diabetes prevalence estimates that just over half a billion people are currently living with DM [2]. Hyperglycemia, dyslipidemia, and insulin resistance, among other metabolic disorders associated with DM, increase the risk of vascular complications [9]. Approximately three out of every four individuals with diabetes will die of cardiovascular disease [71]. Understanding the molecular and cellular mechanisms that link DM to cardiovascular disease will facilitate the development of new therapeutic strategies to treat or prevent disease development.

Previous studies have shown that the accelerated development of atherosclerosis in hyperglycemic apoE$^{-/-}$ mice is associated with reduced vasa vasorum neovascularization [36,37]. It was also observed that vasa vasorum density in the left descending carotid artery, obtained from human autopsies, was significantly lower in individuals who had diabetes compared to non-diabetic individuals [38]. Further analysis revealed that hyperglycemic mice exhibit impaired signalling in the hypoxia-induced angiogenesis pathway. While hyperglycemic mice have increased levels of HIF-1α, a component of the HIF transcription factor involved in increasing angiogenesis, there is no corresponding increase in VEGF or VEGFR2, which are required to promote angiogenesis [36].

In this study, to directly examine the potential role of VEGF in hyperglycemia-induced atherosclerosis, we created a novel atherosclerosis-prone mouse strain that has been genetically modified to permit inducible,

macrophage-specific VEGF overexpression by injecting the small molecule, tamoxifen. The effects of VEGF overexpression on atherosclerosis were examined in normoglycemic and STZ-induced hyperglycemic mice. VEGF overexpression was induced at two different time points during atherosclerotic progression, and vasa vasorum density and components of hypoxia-mediated angiogenesis, HIF-1α, VEGF, and VEGFR2 were quantified. Our hypothesis is that impaired angiogenic signalling contributes to vascular hypoxia and accelerated development of atherosclerosis in hyperglycemia and that the overexpression of a VEGF transgene early in atherogenesis will compensate for the hyperglycemia-associated lack of endogenous VEGF and attenuate lesion development.

5.1 Characterization of the Novel Atherosclerotic Macrophage-Specific Inducible VEGF Mouse Model

To characterize the model, we analyzed the temporal and tissue specificity of tamoxifen-induced VEGF protein expression (**Figure 7**). Six-week-old $VEGF^{tg/0}$CSF1R-$iCRE^{tg/0}apoE^{-/-}$ and $VEGF^{tg/0}apoE^{-/-}$ mice were injected with tamoxifen to investigate the specificity of inducible Cre recombinase expression. A subset of mice $VEGF^{tg/0}$CSF1R-$iCRE^{tg/0}apoE^{-/-}$ mice were injected with corn oil to control for the potential effects of tamoxifen. Thioglycollate elicited peritoneal macrophages, liver and whole heart and aorta were collected from these three

groups 1-, 5- and 9-weeks post-treatment (corresponding to 7, 11 and 15 weeks of age).

Analysis of VEGF protein expression, as quantified by western blot shows a significant increase in VEGF protein expression in peritoneal macrophages one week after tamoxifen treatment compared to both the corn oil and Cre controls (**Figure 9A**). However, there are no significant differences in VEGF protein expression in peritoneal macrophages five or nine weeks after tamoxifen treatment (**Figure 9BC**). These results indicate that VEGF overexpression in macrophages persists for at least one week after tamoxifen injections, possibly after five weeks, and is depleted after nine weeks. This waning of the effect of tamoxifen is expected due to macrophage cell replication. In addition, it is possible that inflammation caused by thioglycollate during peritoneal macrophage collection may have influenced the type of macrophages collected for analysis.

Resident peritoneal macrophages consist of two distinct subpopulations; the majority originate from embryonic precursors and are maintained by self-renewal, and a smaller subset originating from circulating bone marrow-derived monocytes [72–74]. Studies show that following thioglycollate injection, bone marrow-derived inflammatory macrophages are increased [75]. Simultaneously, self-renewing macrophages migrate from the peritoneum to the omentum [73]. This response of peritoneal macrophages to thioglycollate stimuli, in which self-replicating macrophages are reduced and replaced by newly differentiated macrophages, may contribute to our ability to differentiate levels of VEGF

overexpression in our Cre-LOX model. In addition, over time, the percentage of new macrophages that were not present during tamoxifen treatment is expected to increase. Further studies must be completed to increase the sample size and consider the effects of thioglycollate on peritoneal macrophage populations.

VEGF protein expression in liver samples collected from the same mice as the peritoneal macrophages was also analyzed. VEGF protein expressed in liver tissue of the $VEGF^{tg/0}apoE^{-/-}$ control mice was significantly lower than hepatic VEGF protein levels in $VEGF^{tg/0}$CSF1R-$iCRE^{tg/0}apoE^{-/-}$ mice five weeks after tamoxifen or corn oil treatment (**Figure 9E**). This trend is visible but not significant at the one- and nine- week time points (**Figure 9DF**). These results suggest that in the liver, the CSF1R-iCRE gene is sufficient to increase VEGF expression, regardless of tamoxifen treatment. No similar findings have been reported regarding the CSF1R-iCRE gene. It is not clear at this time whether the increase in VEGF protein is a result of expression from the endogenous VEGF gene or the VEGF transgene. Therefore, further characterization of this model, exploring off-target effects in the liver as well as other organs with high and low levels of resident macrophages, is required to elucidate the full effects of this model.

Overall, we have shown that tamoxifen treatment successfully induces a transient VEGF overexpression in macrophages of $VEGF^{tg/0}$CSF1R-$iCRE^{tg/0}apoE^{-/-}$ mice. Furthermore, the diminishing effects of tamoxifen are beneficial to our experimental design as it allows for examination of VEGF

overexpression in early atherosclerosis progression (tamoxifen injections at six weeks age) vs in later atherosclerosis progression (tamoxifen injections at ten weeks age).

5.2 The Effects of VEGF Overexpression on Atherosclerosis of Normoglycemic and Hyperglycemic Mice

To examine the effects of VEGF overexpression on atherosclerosis progression in hyperglycemia, we administered tamoxifen injections to induce transient VEGF overexpression in our $VEGF^{tg/0}$CSF1R-$iCRE^{tg/0}apoE^{-/-}$ mouse model (**Figure 8**). Hyperglycemia was induced in a subset of mice with a series of STZ IP injections. STZ was effective in inducing hyperglycemia compared to the normoglycemic controls (**Table 1** and **Table 2**). Although STZ induces the apoptosis of pancreatic beta cells, pancreas weight to body weight ratios were unaffected in hyperglycemic groups compared to normoglycemic controls (**Figure 10C**). This may be due to the selective necrosis of beta cells in the pancreas, which are one of five cell subtypes in the islets of Langerhans, which only makes up 2% of the pancreas [76].

Both normoglycemic and hyperglycemic mice were treated with one of three tamoxifen treatments. One subset of mice was administered tamoxifen at six weeks of age, another subset at ten weeks, and a subset was administered only corn oil as a vehicle control.

In addition, male and female CSF1R-iCRE$^{tg/0}$apoE$^{-/-}$ mice were enrolled as a genetic control. These mice were administered the citrate buffer control regimen and tamoxifen at six weeks of age.

All mice were harvested at 15 weeks of age, and blood and the whole heart and aorta were collected for further analysis. In addition, liver, perigonadal adipose and pancreas samples were weighed and expressed in terms of a ratio to body weight. To study atherosclerotic development, the aortic arch, where atherosclerotic lesions first develop in mice, was embedded in paraffin and sectioned onto glass slides.

In female mice, hyperglycemia was effective in significantly increasing plaque volume in the absence of tamoxifen (**Figure 12B**). This is consistent with previous research showing that hyperglycemia accelerates the progression of atherosclerosis in apoE$^{-/-}$ mice [36]. There was no effect of tamoxifen on the plaque volume of the normoglycemic groups. In hyperglycemic groups, tamoxifen-induced transient overexpression of VEGF early in atherosclerosis progression (tamoxifen at six weeks of age) was associated with a reduction in plaque volume compared to the corn oil control. In addition, HIF1-α expression, a marker of hypoxia, within the plaques of this group was decreased (**Figure 13**). These results suggest that transient VEGF overexpression in early atherosclerotic development of hyperglycemic female mice effectively reduces atherosclerotic plaque volume and hypoxia within the plaques.

Atherosclerotic plaque was also quantified in hearts collected during the one- and five-weeks after tamoxifen (corresponding to 7- and 11-week-old mice) macrophage and liver collection (**Figure 7**). These samples represent earlier time points of atherosclerosis progression of normoglycemic male and female $VEGF^{tg/0}$CSF1R-i$CRE^{tg/0}apoE^{-/--}$ mice administered tamoxifen or corn oil at six weeks of age. No significant difference in plaque volume is observed in normoglycemic 7- and 11-week-old mice administered tamoxifen at six weeks of age (**Figure 17**). This is expected since no significant differences in plaque volume were observed in male or female normoglycemic mice harvested at 15 weeks of age.

The administration of tamoxifen later in atherosclerosis progression (tamoxifen at ten weeks of age) in hyperglycemic females did not yield any significant results in plaque volume compared to the corn oil control (**Figure 12B**). This suggests that there is a temporal factor in the effectiveness of VEGF overexpression. Perhaps indicating that treatment must be targeted to the early stages of atherosclerosis development. However, since we were not able to show a correlated increase in angiogenesis through vasa vasorum density quantification, the pathway in which VEGF overexpression in macrophages affects early atherosclerotic progression is unclear. In addition, we must consider that since all mice were harvested at the same endpoint at 15 weeks of age, there was more time for tamoxifen injections at six weeks of age to take effect compared to tamoxifen administered at ten weeks of age. Therefore, further

studies should add additional endpoints to test the effectiveness of the tamoxifen treatments over longer periods of time.

No significant differences were noted in the quantification of the atherosclerotic plaque volume in male mice (**Figure 12A**). This may be due to the overall reduced plaque volume in male apoE$^{-/-}$ mice compared to females [63]. An increased sample size may be required to elucidate the more subtle differences in plaque volume. In addition, perhaps different tamoxifen treatment and final harvest time points should be considered for male mice to account for the differences in atherosclerotic progression.

Quantification results of VEGF, VEGFR2 and vasa vasorum density did not yield significant results (**Figure 14-16**). This study did not observe the expected results of significantly reduced VEGF, VEGFR2 and vasa vasorum density in hyperglycemic mice [36]. Further optimization of the immunofluorescence staining and increasing sample size is required to obtain clearer results for this aspect of the analysis.

No significant differences in the measured variables were noted between CSF1R-iCRE$^{tg/0}$apoE$^{-/-}$ mice and treatment-matched VEGF$^{tg/0}$CSF1R-iCRE$^{tg/0}$apoE$^{-/-}$ mice (**Figure 10-16**). This result demonstrated that the VEGF transgene itself does not have any effect on the variables measured.

5.3 Future Directions

In addition to increasing the sample size, further analysis of male mice, optimization of methods for macrophage collection and immunofluorescence staining, and expanding controls, timepoints and endpoints, there are a few other experiments that may be useful in understanding the impaired neovascularization of the vasa vasorum and vascular hypoxia in accelerated development of atherosclerosis in hyperglycemia.

5.3.1 Analyze the Effectiveness of VEGF Secretion by Macrophages Harvested from $VEGF^{tg/0}$CSF1R-$iCRE^{tg/0}apoE^{-/-}$ Mice

Current experimental data suggests tamoxifen effectively increases VEGF expression within peritoneal macrophage cells collected one week after treatment. To confirm the intended effect of VEGF overexpression in atherosclerotic plaques, VEGF expression within lesional macrophages of hearts collected at closer time points to tamoxifen treatment should be analyzed via immunofluorescent staining of serial aortic sections. In addition, for VEGF to be effective in increasing angiogenesis, it must be secreted from the cell to bind to VEGFR2 on the cell surface of other cells. It is important to assess whether VEGF is being released from the cells. Peritoneal macrophages collected from mice one week after tamoxifen injections may be plated and grown ex vivo. Once plated at equal cell densities, cell supernatant may be collected at different time

points to assess the longevity of VEGF release. *In vivo*, systemic circulating VEGF levels should be quantified post-tamoxifen injection at various points.

5.3.2 Investigate Temporal Effects of Tamoxifen in Hyperglycemic VEGF$^{tg/0}$CSF1R-iCRE$^{tg/0}$apoE$^{-/-}$ Mice

Currently, our approach to characterizing the model has only considered normoglycemic mice. Since we have seen a significant difference in the effect of tamoxifen in normoglycemic and hyperglycemic female mice, further analysis into this factor of the mouse model would help elucidate these differences. Analysis of VEGF protein expression in peritoneal macrophages and other organs of tamoxifen treatment and genotype-matched hyperglycemic mice collected one-, five-, and nine-weeks post-treatment would help elucidate the effect of glycemia on VEGF overexpression.

5.3.3 Investigate the Molecular Mechanism by Which Hyperglycemia Impairs VEGF Expression

Examining the effects of regulating glucose concentrations and oxygen availability on HIF-1α and VEGF expression in cultured human THP-1 derived macrophages will elucidate this phenomenon. Western blot may be used to verify hypoxia-associated stabilization of HIF-1α. Reverse transcription quantitative PCR (RT qPCR) and enzyme-linked immunosorbent assay (ELISA) may be used

to analyze the expression and secretion of pro-angiogenic and anti-angiogenic VEGF isoforms. Chromatin immunoprecipitation may be used to investigate the ability of the HIF complex to bind the VEGF promoter.

5.3.4 Investigate the Effects of VEGF Overexpression in a Model of Type 2 DM Mice

The current STZ hyperglycemic model used is generally considered to be a model of Type 1 DM [77]. To better understand the effects of hyperglycemia on atherosclerosis, other mouse models of DM, such as the $Ins2^{Akita}$ and mice fed a high-fat diet, should be utilized [78,79]

5.3.5 Optimize Vasa Vasorum Density Quantification

Identifying vasa vasorum microvessels from serial cross-sections of the aortic sinus is difficult due to the variability in direction of growth of the microvessels and the two-dimensional nature of the sections. The criteria for quantifying vasa vasorum density include a microvessel lumen size cut off of 100μm to assess new microvessel formations. However, microvessels growing perpendicular to the aortic sinus may be sectioned longitudinally, with lumen size appearing to be greater than 100μm, and therefore not quantified as part of vasa vasorum density. A more reliable and efficient way to measure vasa vasorum

structure density and complexity could be achieved using stacked images of thicker tissue samples.

5.4 Limitations

A limitation of the $VEGF^{tg/0}$CSF1R-$iCRE^{tg/0}apoE^{-/-}$ mouse model is that the VEGF overexpression is not only targeted to atherosclerotic plaques, but to all macrophages of the body. Macrophages reside in many tissues, including the lung, spleen, liver, and kidney. Increasing VEGF in other areas of the body may cause effects that could confound the interpretation of these results. Further characterization of these effects could address the extent of this potential issue. At present, there is no way to direct the overexpression of VEGF to lesion macrophages specifically.

Another limitation in this study is the method in which we measured VEGF expression in thioglycollate-elicited macrophages. Thioglycollate is also used as a medium to test the aerotolerance of bacteria as it creates an anerobic environment [80,81]. This property may have affected hypoxia-induced mechanisms in the macrophages, such as HIF1α induced VEGF expression. Since the VEGF antibody used in immunoblotting cannot distinguish between endogenous and transgene VEGF protein, the effects of thioglycollate may have had an effect on the results.

The major assumption of our study is that hyperglycemia impairs vasa vasorum neovascularization. In these studies, we have not investigated other potential effects, such as effects on lymph circulation. This understudied system plays an important role in the movement of lipids and inflammatory cells and could be affected by impaired HIF1α signalling and/or VEGF overexpression.

6. CONCLUSION

People with diabetes are at a 2-4 times higher risk for developing cardiovascular disease than those without. Atherosclerosis, the build-up of plaque in the artery wall, is a major cause of cardiovascular disease. Previous evidence shows that hyperglycemic mice have accelerated atherosclerosis progression, increased hypoxia, inflammation, and expression of hypoxia inducible factor 1 alpha (HIF1-α), a transcription factor for genes involved in angiogenesis. However, impaired signalling through the HIF1-α pathway is evidenced by reduced vascular endothelial growth factor (VEGF), VEGF receptor 2 (VEGFR2) and vasa vasorum density. Our hypothesis is that impaired neovascularization contributes to vascular hypoxia and accelerated development of atherosclerosis in hyperglycemia. To test our hypothesis, we created a novel atherosclerotic macrophage-specific inducible Cre VEGF mouse model to study the effects of VEGF overexpression under normoglycemic and hyperglycemic conditions. Initial characterization of the model showed transient overexpression of VEGF in macrophages lasting at least one week. Our results demonstrate that transient overexpression of VEGF during early atherosclerosis progression reduces plaque volume and hypoxic marker, HIF-1α, in female mice. Further analysis and optimization of techniques are required to expand on and validate these results. Understanding the effects of VEGF expression on lesion development will help delineate the biochemical pathways that link diabetes and cardiovascular

disease. Validation of this mechanism may lead to novel and more effective strategies to treat/prevent diabetic cardiovascular disease (**Figure 18**).

Figure 18: Summary. To examine the effects of VEGF overexpression on atherosclerosis progression in hyperglycemia, we administered tamoxifen to induce transient VEGF overexpression in our $VEGF^{tg/0}$CSF1R-i$CRE^{tg/0}$$apoE^{-/-}$ mouse model. Male and female mice were enrolled at five weeks of age. Hyperglycemia was induced in a subset of mice with a series of STZ IP injections. Tamoxifen injections were used at transiently increase VEGF expression early (6 weeks age) or later (10 weeks age) in the progression of atherosclerosis. At 15 weeks of age, hearts were collected and sectioned at the aortic sinus to analyze plaque volume and immunofluorescence staining of HIF-1α. The results demonstrate that transient overexpression of VEGF during early atherosclerosis progression reduces plaque volume and hypoxic marker, HIF-1α, in female mice.

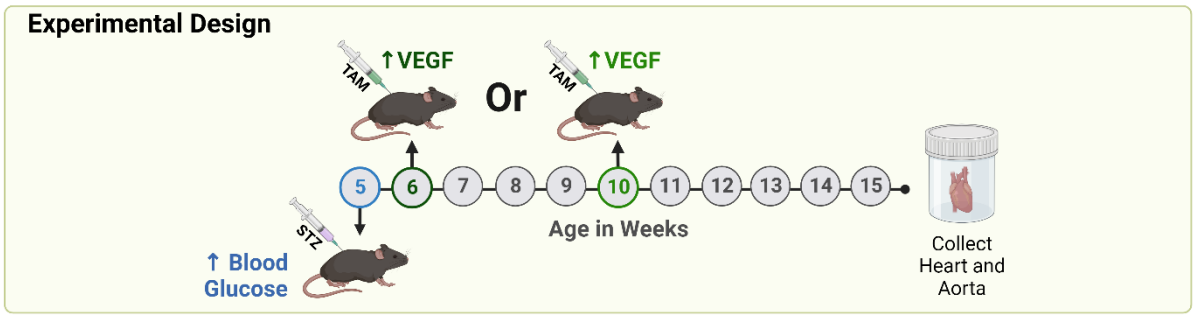
Experimental Design
↑ VEGF
TAM
Or
↑ VEGF
TAM
5
6
7
8
9
10
11
12
13
14
15
Age in Weeks
STZ
↑ Blood Glucose
Collect Heart and Aorta

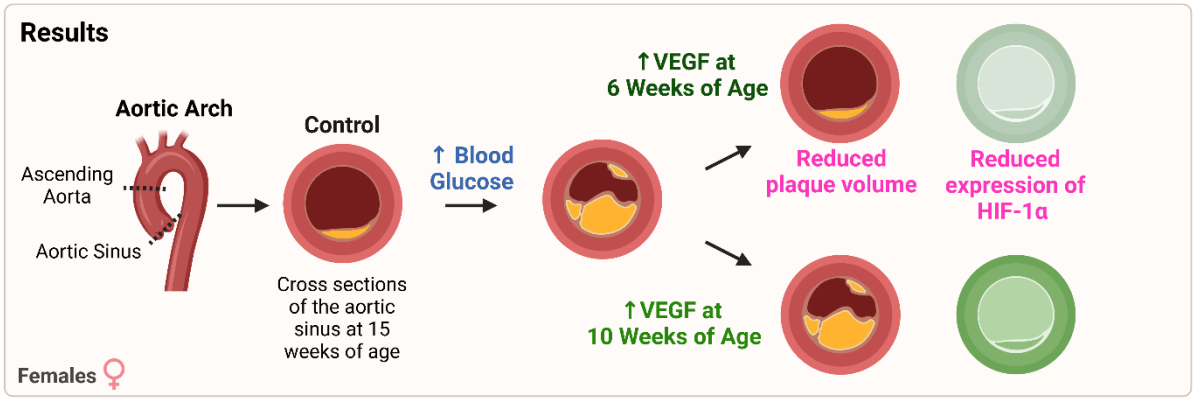
Results
Aortic Arch
Ascending Aorta
Aortic Sinus
Control
Cross sections of the aortic sinus at 15 weeks of age
↑ Blood Glucose
↑ VEGF at 6 Weeks of Age
Reduced plaque volume
Reduced expression of HIF-1α
↑ VEGF at 10 Weeks of Age
Females ♀

7. REFERENCES

[1] Z. Punthakee, R. Goldenberg, P. Katz, Definition, Classification and Diagnosis of Diabetes, Prediabetes and Metabolic Syndrome, Can J Diabetes. 42 (2018) S10–S15. https://doi.org/10.1016/j.jcjd.2017.10.003.

[2] H. Sun, P. Saeedi, S. Karuranga, M. Pinkepank, K. Ogurtsova, B.B. Duncan, C. Stein, A. Basit, J.C.N. Chan, J.C. Mbanya, M.E. Pavkov, A. Ramachandaran, S.H. Wild, S. James, W.H. Herman, P. Zhang, C. Bommer, S. Kuo, E.J. Boyko, D.J. Magliano, IDF Diabetes Atlas: Global, regional and country-level diabetes prevalence estimates for 2021 and projections for 2045, Diabetes Res Clin Pract. 183 (2022). https://doi.org/10.1016/j.diabres.2021.109119.

[3] Diabetes Canada, Diabetes in Canada: Backgrounder, (2020).

[4] Cardiovascular disease and risk management, Diabetes Care. 40 (2017) S75–S87. https://doi.org/10.2337/dc17-S012.

[5] 2. Classification and diagnosis of diabetes, Diabetes Care. 38 (2015) S8–S16. https://doi.org/10.2337/dc15-S005.

[6] T. Tuomi, N. Santoro, S. Caprio, M. Cai, J. Weng, L. Groop, The many faces of diabetes: A disease with increasing heterogeneity, The Lancet. 383 (2014) 1084–1094. https://doi.org/10.1016/S0140-6736(13)62219-9.

[7] G. Wilcox, Insulin and Insulin Resistance, Clin Biochem Rev. 26 (2005) 19–39.

[8] R.A. DeFronzo, Pathogenesis of type 2 diabetes mellitus, Medical Clinics of North America. 88 (2004) 787–835. https://doi.org/10.1016/j.mcna.2004.04.013.

[9] E. Bonora, R.A. DeFronzo, Diabetes Complications, Comorbidities and Related Disorders, 2nd ed., Springer International Publishing, 2020. https://doi.org/10.1007/978-3-030-36694-0.

[10] Y. Nakashima, A.S. Plump, E.W. Raines, J.L. Breslow, R. Ross, ApoE-Deficient Mice Develop Lesions of All Phases of Atherosclerosis Throughout the Arterial Tree, Atherosclerosis and Thrombosis. 14 (1994) 133–140.

[11] A.J. Lusis, Atherosclerosis - Insight Review Articles, Nature. 407 (2000) 233–241.

[12] S. Haffner, S. Lehto, T. Ronnemaa, K. Pyorala, M. Laakso, Mortality from coronary heart disease in subjects with type2 diabetes and in nondiabetic subjects with and without prior myocardial infarction., N Engl J Med. 339 (1998) 229–234.

[13] S. Vigili de Kreutzenberg, A. Coracina, A. Volpi, G.P. Fadini, A.C. Frigo, G. Guarneri, A. Tiengo, A. Avogaro, Microangiopathy is independently

associated with presence, severity and composition of carotid atherosclerosis in type 2 diabetes, Nutrition, Metabolism and Cardiovascular Diseases. 21 (2011) 286–293. https://doi.org/10.1016/j.numecd.2009.10.003.

[14] R.S. Rosenson, P. Fioretto, P.M. Dodson, Does microvascular disease predict macrovascular events in type two diabetes?, Atherosclerosis. 218 (2011) 13–18.

[15] M. Brownlee, The Pathobiology of Diabetic Complications A Unifying Mechanism, Diabetes. 54 (2005) 1615–1625. http://diabetesjournals.org/diabetes/article-pdf/54/6/1615/381945/zdb00605001615.pdf.

[16] N. Katakami, Mechanism of development of atherosclerosis and cardiovascular disease in diabetes mellitus, J Atheroscler Thromb. 25 (2018) 27–39. https://doi.org/10.5551/jat.RV17014.

[17] G. Orasanu, J. Plutzky, The Pathologic Continuum of Diabetic Vascular Disease, J Am Coll Cardiol. 53 (2009). https://doi.org/10.1016/j.jacc.2008.09.055.

[18] A. Poznyak, A. v. Grechko, P. Poggio, V.A. Myasoedova, V. Alfieri, A.N. Orekhov, The diabetes mellitus–atherosclerosis connection: The role of lipid and glucose metabolism and chronic inflammation, Int J Mol Sci. 21 (2020). https://doi.org/10.3390/ijms21051835.

[19] F. Paneni, J.A. Beckman, M.A. Creager, F. Cosentino, Diabetes and vascular disease: Pathophysiology, clinical consequences, and medical therapy: Part i, Eur Heart J. 34 (2013) 2436–2446. https://doi.org/10.1093/eurheartj/eht149.

[20] Z. Ming Dong, S.M. Chapman, A.A. Brown, P.S. Frenette, R.O. Hynes, D.D. Wagner, The Combined Role of P-and E-Selectins in Atherosclerosis, Journal of Clinical Investigation. 102 (1998) 145–152. http://www.jci.org.

[21] A.D. Watson, N. Leitinger, M. Navab, K.F. Faull, S. Hörkkö, J.L. Witztum, W. Palinski, D. Schwenke, R.G. Salomon, W. Sha, G. Subbanagounder, A.M. Fogelman, J.A. Berliner, Structural identification by mass spectrometry of oxidized phospholipids in minimally oxidized low density lipoprotein that induce monocyte/endothelial interactions and evidence for their presence in vivo, Journal of Biological Chemistry. 272 (1997) 13597–13607. https://doi.org/10.1074/jbc.272.21.13597.

[22] P. Tontonoz, L. Nagy, J.G.A. Alvarez, V.A. Thomazy, R.M. Evans, PPAR gamma Promotes Monocyte/Macrophage Differentiation and Uptake of Oxidized LDL, Cell. 93 (1998) 241–252.

[23] Ross Russell, The pathogenesis of atherosclerosis: a perspective for the 1990s, Nature. 362 (1993) 801.

[24] E.A. Podrez, M. Febbraio, N. Sheibani, D. Schmitt, R.L. Silverstein, D.P. Hajjar, P.A. Cohen, W.A. Frazier, H.F. Hoff, S.L. Hazen, Macrophage

scavenger receptor CD36 is the major receptor for LDL modified by monocyte-generated reactive nitrogen species, Journal of Clinical Investigation. 105 (2000) 1095–1108. https://doi.org/10.1172/JCI8574.

[25] D.N. Streblow, C. Soderberg-Naucler, J. Vieira, P. Smith, E. Wakabayashi, F. Ruchti, K. Mattison, Y. Altschuler, J.A. Nelson, The Human Cytomegalovirus Chemokine Receptor US28 Mediates Vascular Smooth Muscle Cell Migration, Cell. 99 (1999) 511–520.

[26] I. Tabas, Consequences and therapeutic implications of macrophage apoptosis in atherosclerosis: The importance of lesion stage and phagocytic efficiency, Arterioscler Thromb Vasc Biol. 25 (2005) 2255–2264. https://doi.org/10.1161/01.ATV.0000184783.04864.9f.

[27] L. Fernández-Friera, V. Fuster, B. López-Melgar, B. Oliva, J.M. García-Ruiz, J. Mendiguren, H. Bueno, S. Pocock, B. Ibáñez, A. Fernández-Ortiz, J. Sanz, Normal LDL-Cholesterol Levels Are Associated With Subclinical Atherosclerosis in the Absence of Risk Factors, J Am Coll Cardiol. 70 (2017) 2979–2991. https://doi.org/10.1016/j.jacc.2017.10.024.

[28] T. Björnheden, M. Levin, M. Evaldsson, O. Wiklund, Evidence of hypoxic areas within the arterial wall in vivo, Arterioscler Thromb Vasc Biol. 19 (1999) 870–876. https://doi.org/10.1161/01.ATV.19.4.870.

[29] L.S. Athanasiou, D.I. Fotiadis, L.K. Michalis, Chapter 1: Introduction, in: Atherosclerotic Plaque Characterization Methods Based on Coronary

Imaging, 2017: pp. 1–21. https://doi.org/10.1016/b978-0-12-804734-7.00001-4.

[30] E.L. Ritman, A. Lerman, The dynamic vasa vasorum, Cardiovasc Res. 75 (2007) 649–658. https://doi.org/10.1016/j.cardiores.2007.06.020.

[31] M.J. Mulligan-Kehoe, M. Simons, Vasa vasorum in normal and diseased arteries, Circulation. 129 (2014) 2557–2566. https://doi.org/10.1161/CIRCULATIONAHA.113.007189.

[32] D.G. Sedding, E.C. Boyle, J.A.F. Demandt, J.C. Sluimer, J. Dutzmann, A. Haverich, J. Bauersachs, Vasa vasorum angiogenesis: Key player in the initiation and progression of atherosclerosis and potential target for the treatment of cardiovascular disease, Front Immunol. 9 (2018). https://doi.org/10.3389/fimmu.2018.00706.

[33] T.G. Kwon, L.O. Lerman, A. Lerman, The vasa vasorum in atherosclerosis: The vessel within the vascular wall, J Am Coll Cardiol. 65 (2015) 2478–2480. https://doi.org/10.1016/j.jacc.2015.04.032.

[34] S.H. Wilson, J. Herrmann, L.O. Lerman, D.R. Holmes, C. Napoli, E.L. Ritman, A. Lerman, Simvastatin preserves the structure of coronary adventitial vasa vasorum in experimental hypercholesterolemia independent of lipid lowering, Circulation. 105 (2002) 415–418. https://doi.org/10.1161/hc0402.104119.

[35] F. Kuwahara, H. Kai, K. Tokuda, R. Shibata, K. Kusaba, N. Tahara, H. Niiyama, T. Nagata, T. Imaizumi, Hypoxia-inducible factor-1α/vascular endothelial growth factor pathway for adventitial vasa vasorum formation in hypertensive rat aorta, Hypertension. 39 (2002) 46–50. https://doi.org/10.1161/hy1201.097200.

[36] K.J. Veerman, D.E. Venegas-Pino, Y. Shi, M.I. Khan, H.C. Gerstein, G.H. Werstuck, Hyperglycaemia is associated with impaired vasa vasorum neovascularization and accelerated atherosclerosis in apolipoprotein-E deficient mice, Atherosclerosis. 227 (2013) 250–258. https://doi.org/10.1016/j.atherosclerosis.2013.01.018.

[37] L.H. Zhong, A. Bruton, C. Araja, V. Dang, Y. Shi, G.H. Werstuck, Arterial Wall Hypoxia Promotes Atherosclerosis in Hyperglycemic Apolipoprotein E-De fi cient Mice, International Journal of Cardiovascular Diseases & Diagnosis. 5 (2020) 3–10.

[38] H.C. Gerstein, V. Nair, R. Chaube, H. Stoute, G. Werstuck, Dysglycemia and the density of the coronary vasa vasorum, Diabetes Care. 42 (2019) 980–982. https://doi.org/10.2337/dc18-2483.

[39] M. Soleimani, A. Haverich, P. Wriggers, Mathematical Modeling and Numerical Simulation of Atherosclerosis Based on a Novel Surgeon's View, Archives of Computational Methods in Engineering. 28 (2021) 4263–4282. https://doi.org/10.1007/s11831-021-09623-5.

[40] D. Pirri, M. Fragiadaki, P.C. Evans, Diabetic atherosclerosis: Is there a role for the hypoxia-inducible factors?, Biosci Rep. 40 (2020) 1–12. https://doi.org/10.1042/BSR20200026.

[41] J.-W. Lee, S.-H. Bae, J.-W. Jeong, S.-H.S.-H.K. Kim, K.-W. Kim, Hypoxia-inducible facotr (HIF-1)a: its protein stability and biological functions, Exp Mol Med. 36 (2004) 1–12.

[42] L. Gao, Q. Chen, X. Zhou, L. Fan, The role of hypoxia-inducible factor 1 in atherosclerosis, J Clin Pathol. 65 (2012) 872–876. https://doi.org/10.1136/jclinpath-2012-200828.

[43] J.A. Nagy, A.M. Dvorak, H.F. Dvorak, VEGF-A and the induction of pathological angiogenesis, Annu Rev Pathol. 2 (2007) 251–275. https://doi.org/10.1146/annurev.pathol.2.010506.134925.

[44] H. Takahashi, M. Shibuya, The vascular endothelial growth factor (VEGF)/VEGF receptor system and its role under physiological and pathological conditions, Clin Sci. 109 (2005) 227–241. https://doi.org/10.1042/CS20040370.

[45] S.J. Harper, D.O. Bates, VEGF-A splicing : the key to anti-angiogenic therapeutics?, Nat Rev Cancer. 8 (2008) 880–887. https://doi.org/10.1038/nrc2505.

[46] S. Chen, F.N. Ziyadeh, Vascular endothelial growth factor and diabetic nephropathy, Curr Diab Rep. 8 (2008) 470–476. https://doi.org/10.1007/s11892-008-0081-3.

[47] E. Chou, I. Suzuma, K.J. Way, D. Opland, A.C. Clermont, K. Naruse, K. Suzuma, N.L. Bowling, C.J. Vlahos, L.P. Aiello, G.L. King, Decreased cardiac expression of vascular endothelial growth factor and its receptors in insulin-resistant and diabetic states: A possible explanation for impaired collateral formation in cardiac tissue, Circulation. 105 (2002) 373–379. https://doi.org/10.1161/hc0302.102143.

[48] D. Cervi, Y. Shaked, M. Haeri, T. Usenko, C.R. Lee, J.J. Haigh, A. Nagy, R.S. Kerbel, E. Yefenof, Y. Ben-David, Enhanced natural-killer cell and erythropoietic activities in VEGF-A-overexpressing mice delay F-MuLV-induced erythroleukemia, Blood. 109 (2007) 2139–2146. https://doi.org/10.1182/blood-2005-11-026823.

[49] Y. Wang, E. Kilic, Ü. Kilic, B. Weber, C.L. Bassetti, H.H. Marti, D.M. Hermann, VEGF overexpression induces post-ischaemic neuroprotection, but facilitates haemodynamic steal phenomena, Brain. 128 (2005) 52–63. https://doi.org/10.1093/brain/awh325.

[50] E. Pinter, J. Haigh, A. Nagy, J.A. Madri, Hyperglycemia-induced vasculopathy in the murine conceptus is mediated via reductions of VEGF-A expression and VEGF receptor activation, American Journal of

Pathology. 158 (2001) 1199–1206. https://doi.org/10.1016/S0002-9440(10)64069-2.

[51] M.I. Dorrell, E. Aguilar, R. Jacobson, S.A. Trauger, J. Friedlander, G. Siuzdak, M. Friedlander, Maintaining retinal astrocytes normalizes revascularization and prevents vascular pathology associated with oxygen-induced retinopathy, Glia. 58 (2010) 43–54. https://doi.org/10.1002/glia.20900.

[52] N. Gupta, S. Mansoor, A. Sharma, A. Sapkal, J. Sheth, P. Falatoonzadeh, B. Kuppermann, M. Kenney, Diabetic Retinopathy and VEGF, Open Ophthalmol J. 7 (2013) 4–10. https://doi.org/10.2174/1874364101307010004.

[53] A.S. De Vriese, R.G. Tilton, M. Elger, C.C. Stephan, W. Kriz, N.H. Lameire, Antibodies against vascular endothelial growth factor improve early renal dysfunction in experimental diabetes, Journal of the American Society of Nephrology. 12 (2001) 993–1000.

[54] G. Lo Sasso, W.K. Schlage, S. Boué, E. Veljkovic, M.C. Peitsch, J. Hoeng, The Apoe-/- mouse model: A suitable model to study cardiovascular and respiratory diseases in the context of cigarette smoke exposure and harm reduction, J Transl Med. 14 (2016) 1–16. https://doi.org/10.1186/s12967-016-0901-1.

[55] S.H. Zhang, R.L. Reddick, J.A. Piedrahita, N. Maeda, Spontaneous Hypercholesterolemia and Arterial Lesions in Mice Lacking Apolipoprotein E, Science (1979). 258 (1992) 468–471. https://doi.org/10.1126/science.1411543.

[56] S.A. Dabravolski, V.A. Khotina, A. v. Omelchenko, V.A. Kalmykov, A.N. Orekhov, The Role of the VEGF Family in Atherosclerosis Development and Its Potential as Treatment Targets, Int J Mol Sci. 23 (2022). https://doi.org/10.3390/ijms23020931.

[57] C. Silvestre-Roig, P. Lemnitzer, J. Gall, S. Schwager, A. Toska, L. Yvan-Charvet, M. Detmar, O. Soehnlein, Arterial Delivery of VEGF-C Stabilizes Atherosclerotic Lesions, Circ Res. 128 (2021) 284–286. https://doi.org/10.1161/CIRCRESAHA.120.317186.

[58] S. Karaman, M. Hollmén, S.Y. Yoon, H.F. Alkan, K. Alitalo, C. Wolfrum, M. Detmar, Transgenic overexpression of VEGF-C induces weight gain and insulin resistance in mice, Sci Rep. 6 (2016) 1–12. https://doi.org/10.1038/srep31566.

[59] D. Yan, D. Zhang, L. Lu, H. Qiu, J. Wang, Vascular endothelial growth factor-modified macrophages accelerate reendothelialization and attenuate neointima formation after arterial injury in atherosclerosis-prone mice, J Cell Biochem. 120 (2019) 10652–10661. https://doi.org/10.1002/jcb.28355.

[60] A.S. Plump, J.L. Breslow, Apolipoprotein E and the Apolipoprotein E-deficient Mouse, Annu Rev Nutr. 15 (1995) 495–518. https://doi.org/10.1038/375285b0.

[61] S. Fazio, V.R. Babaev, A.B. Murray, A.H. Hasty, K.J. Carter, L.A. Gleaves, J.B. Atkinson, M.F. Linton, Increased atherosclerosis in mice reconstituted with apolipoprotein E null macrophages, Proc Natl Acad Sci U S A. 94 (1997) 4647–4652. https://doi.org/10.1073/pnas.94.9.4647.

[62] Jax Laboraotry, B6.129P2-Apoe tm1Unc/J, (n.d.). https://www.jax.org/strain/002052 (accessed January 13, 2021).

[63] D.D. Smith, X. Tan, O. Tawfik, G. Milne, D.J. Stechschulte, K.N. Dileepan, Increased aortic atherosclerotic plaque development in female apolipoprotein E-null mice is associated with elevated thromboxane A2 and decreased prostacyclin production, Journal of Physiology and Pharmacology. 61 (2010) 309–316.

[64] J.A. Piedrahita, S.H. Zhang, J.R. Hagaman, P.M. Oliver, N. Maeda, Generation of mice carrying a mutant apolipoprotein E gene inactivated by gene targeting in embryonic stem cells, Proc Natl Acad Sci U S A. 89 (1992) 4471–4475. https://doi.org/10.1073/pnas.89.10.4471.

[65] C. Maes, S. Goossens, S. Bartunkova, B. Drogat, L. Coenegrachts, I. Stockmans, K. Moermans, O. Nyabi, K. Haigh, M. Naessens, L. Haenebalcke, J.P. Tuckermann, M. Tjwa, P. Carmeliet, V. Mandic, J.P.

David, A. Behrens, A. Nagy, G. Carmeliet, J.J. Haigh, Increased skeletal VEGF enhances B-catenin activity and results in excessively ossified bones, EMBO Journal. 29 (2010) 424–441. https://doi.org/10.1038/emboj.2009.361.

[66] V.T. Chu, T. Weber, R. Graf, T. Sommermann, K. Petsch, U. Sack, P. Volchkov, K. Rajewsky, R. Kühn, Efficient generation of Rosa26 knock-in mice using CRISPR/Cas9 in C57BL/6 zygotes, BMC Biotechnol. 16 (2016) 1–15. https://doi.org/10.1186/s12896-016-0234-4.

[67] Jax Laboraotry, Tg(Csf1r-cre/Esr1*)1Jwp/J, (n.d.). https://www.jax.org/strain/019098 (accessed January 17, 2021).

[68] B. Constanze, D.A. Hume, The transcriptional regulation of the Colony-Stimulating Factor 1 Receptor (csf1r) gene during hemotopoiesis, Frontiers in Bioscience. 13 (2008) 549–560.

[69] S. Lenzen, The mechanisms of alloxan- and streptozotocin-induced diabetes, Diabetologia. 51 (2008) 216–226. https://doi.org/10.1007/s00125-007-0886-7.

[70] D.E. Venegas-Pino, N. Banko, M.I. Khan, Y. Shi, G.H. Werstuck, Quantitative analysis and characterization of atherosclerotic lesions in the murine aortic sinus., J Vis Exp. (2013) 50933. https://doi.org/10.3791/50933.

[71] C. Triplitt, C.A. Alvarez, Best Practices for Lowering the Risk of CVD in DM, Diabetes Spectrum. 21 (2008) 177–189.

[72] A.A. Cassado, M.R. D'Império Lima, K.R. Bortoluci, Revisiting mouse peritoneal macrophages: Heterogeneity, development, and function, Front Immunol. 6 (2015). https://doi.org/10.3389/fimmu.2015.00225.

[73] E.E. Bou Ghosn, A.A. Cassado, G.R. Govoni, T. Fukuhara, Y. Yang, D.M. Monack, K.R. Bortoluci, S.R. Almeida, L.A. Herzenberg, L.A. Herzenberg, Two physically, functionally, and developmentally distinct peritoneal macrophage subsets, Proc Natl Acad Sci U S A. 107 (2010) 2568–2573. https://doi.org/10.1073/pnas.0915000107.

[74] D.W. Cain, E.G. O'Koren, M.J. Kan, M. Womble, G.D. Sempowski, K. Hopper, M.D. Gunn, G. Kelsoe, Identification of a Tissue-Specific, C/EBPβ-Dependent Pathway of Differentiation for Murine Peritoneal Macrophages, The Journal of Immunology. 191 (2013) 4665–4675. https://doi.org/10.4049/jimmunol.1300581.

[75] L.C. Davies, M. Rosas, S.J. Jenkins, C. te Liao, M.J. Scurr, F. Brombacher, D.J. Fraser, J.E. Allen, S.A. Jones, P.R. Taylor, Distinct bone marrow-derived and tissue-resident macrophage lineages proliferate at key stages during inflammation, Nat Commun. 4 (2013). https://doi.org/10.1038/ncomms2877.

[76] Y. El-Gohary, G. Gittes, Structure of Islets and Vascular Relationship to the Exocrine Pancreas, Pancreapedia. (2018). https://doi.org/10.3998/panc.2017.10.

[77] T.L. van Belle, P. Taylor, M.G. von Herrath, Mouse models for Type 1 Diabetes, Drug Discov Today Dis Models. 6 (2009) 41–45. https://doi.org/10.1016/j.ddmod.2009.03.008.

[78] E.-G. Hong, D. Young Jung, H. Jin Ko, Z. Zhang, Z. Ma, J.Y. Jun, J. Hyeong Kim, A.D. Sumner, T.C. Vary, T.W. Gardner, S.K. Bronson, J.K. Kim, H. E-g, Nonobese, insulin-deficient Ins2 Akita mice develop type 2 diabetes phenotypes including insulin resistance and cardiac remodeling, Am J Physiol Endocrinol Metab. 293 (2007) 1687–1696. https://doi.org/10.1152/ajpendo.00256.2007.-Although.

[79] A.J. King, The use of animal models in diabetes research, Br J Pharmacol. 166 (2012) 877–894. https://doi.org/10.1111/(ISSN)1476-5381/homepage/animal_models.htm.

[80] D. Karakashev, D. Galabova, I. Simeonov, A simple and rapid test for differentiation of aerobic from anaerobic bacteria, World J Microbiol Biotechnol. 19 (2003) 233–238.

[81] N.G. Sakhno, O. v. Gunar, M. v. Roshchina, L. v. Kolosova, V. Grigor'eva, Isolation of Anaerobic Bacteria During Quality Analysis of Medicinal

Products, Pharm Chem J. 52 (2018) 569–572.

https://doi.org/10.1007/s11094-018-1861-y.